

UNIVERSITY OF PRETORIA

Faculty of Engineering, Built Environment and Information Technology

*Department of Mechanical and Aeronautical Engineering*

# THE INFLUENCE OF A MULTIPLE TUBE INLET CONDITION ON HEAT TRANSFER IN THE TRANSITIONAL FLOW REGIME

Dissertation by

Leslie Matthew James Pallent

Submitted in fulfilment of the requirements for the degree of  
**MASTER OF ENGINEERING**

JULY 2017

SUPERVISOR: PROFESSOR J.P. MEYER

## ABSTRACT

Title: The influence of a multiple tube inlet condition on heat transfer in the transitional flow regime.

Author: Leslie Matthew James Pallent

Supervisor: Prof J.P. Meyer

Faculty: Engineering, Built Environment and Information Technology

Department: Mechanical and Aeronautical Engineering

Degree: Master of Engineering (Mechanical Engineering)

In the industrial design of heat exchangers, engineers have long followed the general rule of avoiding transitional flow, and have rather designed a system operating in the turbulent flow regime. Whilst the turbulent regime is better for heat transfer, the higher friction inside the tube results in a much higher pressure drop which inevitably results in the system requiring a more powerful pump than if the system were to operate in the laminar regime. Designing a heat exchanger that operates in the turbulent flow regime is often the safer option, since little published design data is available for flow in the transitional flow regime, giving rise to numerous unwanted uncertainties during the design phase. Recent research into the transitional flow regime has resulted in promising experimental data that shows the regime is not as unstable as previously suspected. The regime allows for higher heat transfer than flows in the laminar regime, yet lower pressure drops than flows in the turbulent regime. Numerous investigations have previously been performed on a single uniformly heated tube operating in the transitional flow regime, however, there exists no data on the influence of a multiple tube inlet condition, as typically found in shell and tube heat exchangers, on the heat transfer characteristics. The purpose of this study was thus to determine the influence of varying tube pitch ratios on the fully developed heat transfer characteristics of three smooth circular horizontal tubes. An experimental set up was designed and built to accommodate a single tube heat exchanger used for validation purposes, and a multiple tube heat exchanger comprising of three identical and equally spaced tubes. Using a DC power supply, the tubes were uniformly heated at 2, 3 and 4 kW/m<sup>2</sup> along the length of the test section. The heat transfer characteristics were determined experimentally for outer diameter tube pitch ratios of 1.25 and 1.5 of three 4 mm inner diameter tubes, each 6 m in length for a range of Reynolds numbers of 1 000 to 7 000. Water was used as the test fluid. Using PT100 probes and thermocouples at the inlet, outlet and outer surface of the test section, it was found that the presence of multiple tubes at the inlet of the heat exchanger for a pitch ratio of 1.25 promoted the onset of transition for the centre tube, and sharpened the transition gradient of the outer tubes. This effect noticeably increased with increasing heat flux and was absent at the higher pitch ratio of 1.5.

## ACKNOWLEDGEMENTS

The success of this investigation would not have been possible without the help and support of the following individuals:

1. Prof Josua Meyer, for his extensive knowledge in the field and for his guidance throughout the course of the investigation as my supervisor.
2. Mr. Danie Gouws, for his support and advice on the technical aspects of the project.
3. Ms. Marilize Everts, for her guidance, support and experience.
4. Mr. Martin Joubert, friend and fellow researcher, for his support, hard work and manufacturing experience.
5. Ms. Laura Leeming for her continuous moral support and motivation.

I would also like to thank the following institutions for their financial support:

- NRF & DST.
- University of Pretoria CERG.

# TABLE OF CONTENTS

<b>Abstract</b> .....	<b>i</b>
<b>Acknowledgements</b> .....	<b>ii</b>
<b>List of Figures and Tables</b> .....	<b>vi</b>
<b>Nomenclature</b> .....	<b>viii</b>
<b>1. Introduction</b> .....	<b>1</b>
1.1 Background.....	1
1.2 Problem statement.....	3
1.3 Objectives.....	3
1.4 Scope of work.....	3
1.5 Content of report.....	3
<b>2. Literature Study</b> .....	<b>4</b>
2.1 Introduction.....	4
2.2 Non-dimensional parameters.....	4
2.2.1 Reynolds number.....	4
2.2.2 Nusselt number.....	4
2.2.3 Prandtl number.....	4
2.2.4 Grashof number.....	4
2.2.5 Rayleigh number.....	5
2.3 Classification of fluid flow.....	5
2.3.1 Factors influencing the flow regime.....	5
2.4 The entrance region.....	5
2.4.1 Hydrodynamic entrance region.....	6
2.4.2 Thermal entrance region.....	6
2.4.3 Entry lengths.....	7
2.4.4 Types of inlets.....	7
2.5 Fundamentals of heat transfer.....	7
2.5.1 Boundary conditions.....	7
2.5.2 Forms of heat transfer.....	9
2.6 Shell-and-tube heat exchangers.....	10
2.6.1 Tube configuration.....	10
2.6.2 Flow maldistribution.....	11
2.7 Previous work.....	11
2.7.1 Work of Ghajar.....	12



2.7.2	Work of Meyer .....	12
2.7.3	Shortcomings of previous work.....	13
2.8	Conclusion.....	13
<b>3.</b>	<b>Experimental Set-up.....</b>	<b>14</b>
3.1	Introduction .....	14
3.2	Experimental set-up.....	14
3.3	Calming section .....	15
3.4	Test section.....	16
3.5	Mixing section.....	17
3.5.1	Manifold.....	17
3.6	Instrumentation.....	18
3.6.1	Power supply.....	18
3.6.2	Flow meters .....	18
3.6.3	RTD probes .....	18
3.6.4	Data acquisition.....	18
3.7	Data reduction .....	18
3.7.1	Energy balance .....	18
3.7.2	Temperature .....	19
3.7.3	Reynolds number.....	20
3.7.4	Heat transfer parameters .....	20
3.8	Experimental procedure.....	20
3.9	Uncertainty.....	21
3.9.1	Equipment uncertainty .....	21
3.9.2	Fluid property uncertainty .....	22
3.9.3	Calculated uncertainties.....	22
3.10	Conclusion.....	24
<b>4.</b>	<b>Validation.....</b>	<b>26</b>
4.1	Introduction .....	26
4.2	Average Nusselt number .....	26
4.3	Local Nusselt number.....	27
4.4	Conclusion.....	28
<b>5.</b>	<b>Results.....</b>	<b>29</b>
5.1	Introduction .....	29
5.2	Laminar and turbulent heat transfer results for a pitch of 1.5 .....	29
5.2.1	2 kW/m <sup>2</sup> heat flux.....	29



5.2.2	3 kW/m <sup>2</sup> heat flux.....	30
5.2.3	4 kW/m <sup>2</sup> heat flux.....	31
5.3	Transitional heat transfer results for a pitch of 1.5 .....	32
5.3.1	2 kW/m <sup>2</sup> heat flux.....	32
5.3.2	3 kW/m <sup>2</sup> heat flux.....	33
5.3.3	4 kW/m <sup>2</sup> heat flux.....	34
5.4	Laminar and turbulent heat transfer results for a pitch of 1.25 .....	35
5.4.1	2 kW/m <sup>2</sup> heat flux.....	35
5.4.2	3 kW/m <sup>2</sup> heat flux.....	36
5.4.3	4 kW/m <sup>2</sup> heat flux.....	36
5.5	Transitional heat transfer results for a pitch of 1.25 .....	37
5.5.1	2 kW/m <sup>2</sup> heat flux.....	37
5.5.2	3 kW/m <sup>2</sup> heat flux.....	38
5.5.3	4 kW/m <sup>2</sup> heat flux.....	39
5.6	Comparison of results.....	41
5.7	Conclusion.....	41
<b>6.</b>	<b>Summary, conclusions and recommendations .....</b>	<b>43</b>
6.1	Summary .....	43
6.2	Conclusions.....	43
6.3	Recommendations.....	44
	<b>References .....</b>	<b>45</b>
<b>Appendix A</b>	<b>Calibration.....</b>	<b>A-1</b>
<b>Appendix B</b>	<b>Uncertainty .....</b>	<b>B-1</b>

## LIST OF FIGURES AND TABLES

Figure 2.1. Injection of dye into a stream to visualise flow regimes. ....	5
Figure 2.2. The hydrodynamic entry length. ....	6
Figure 2.3. The thermal entry length. ....	6
Figure 2.4. The four inlet geometries. ....	7
Figure 2.5. Surface ( $T_s$ ), inlet ( $T_i$ ) and outlet ( $T_o$ ) fluid temperature for the uniform heat flux boundary condition. ....	8
Figure 2.6. Surface ( $T_s$ ), inlet ( $T_i$ ) and outlet ( $T_o$ ) fluid temperature for the constant wall temperature boundary condition. ....	8
Figure 2.7. Secondary flow within the tube cross-section. ....	9
Figure 2.8. A simple shell-and-tube heat exchanger. ....	10
Figure 2.9. Shell-and-tube heat exchanger tube configuration – square (left) and triangular (right). ...	10
Figure 3.1. Schematic representation of the experimental set-up showing the multiple tube arrangement. ....	14
Figure 3.2. Cross-sectional view of the calming section showing screen inserts and the mechanical seal. Dimensions in [mm]. ....	15
Figure 3.3. Cross-sectional view of the tube showing thermocouple orientations (left) and the alternating manner in which thermocouples B and D were attached (right). ....	16
Figure 3.4. Axial locations of the thermocouple stations showing a concentration of stations in the fully developed region. ....	17
Figure 3.5. The mixer block designed to ensure accurate measurement of the fluid bulk outlet temperature. ....	17
Figure 3.6. The uncertainty for Reynolds number at a pitch of 1.5 for 2, 3 and 4 kW/m <sup>2</sup> are given in (a), (b) and (c) respectively and the uncertainty at a pitch of 1.25 for 2, 3 and 4 kW/m <sup>2</sup> are given in (d), (e) and (f) respectively. ....	22
Figure 3.7. The uncertainty for Nusselt number at a pitch of 1.5 for 2, 3 and 4 kW/m <sup>2</sup> is given in (a), (b) and (c) respectively and the uncertainty at a pitch of 1.25 for 2, 3 and 4 kW/m <sup>2</sup> is given in (d), (e) and (f) respectively. ....	24
Figure 3.8. The uncertainty for Colburn $j$ -factor at a pitch of 1.5 for 2, 3 and 4 kW/m <sup>2</sup> is given in (a), (b) and (c) respectively and the uncertainty at a pitch of 1.25 for 2, 3 and 4 kW/m <sup>2</sup> is given in (d), (e) and (f) respectively. ....	24
Figure 4.1. Comparison of average Nusselt number for the single tube for fully developed flow at a heat flux of 4 kW/m <sup>2</sup> with correlations available in literature. ....	26
Figure 4.2. Average Nusselt number vs Reynolds number plot for a heat flux of 1 kW/m <sup>2</sup> showing the critical Reynolds number before the flow enters the transitional regime. ....	27
Figure 4.3. Local Nusselt number vs $x/D_i$ plot for a heat flux of 1 kW/m <sup>2</sup> at a Reynolds number of 2 109 showing the length of the thermal entry region and the convergence to the theoretical Nusselt number of 4.36. ....	28
Figure 5.1. Average Nusselt number (top) and Colburn $j$ -factor (bottom) plotted against Reynolds number for the single and three-tube set-up for a heat flux of 2 kW/m <sup>2</sup> and a pitch of 1.5. ....	30
Figure 5.2. Average Nusselt number (top) and Colburn $j$ -factor (bottom) plotted against Reynolds number for the single and three-tube set-up for a heat flux of 3 kW/m <sup>2</sup> and a pitch of 1.5. ....	30
Figure 5.3. Average Nusselt number (top) and Colburn $j$ -factor (bottom) plotted against Reynolds number for the single and three-tube set-up for a heat flux of 4 kW/m <sup>2</sup> and a pitch of 1.5. ....	31
Figure 5.4. Transitional average Nusselt number (top) and Colburn $j$ -factor (bottom) plotted against Reynolds number for the single and three-tube set-up for a heat flux of 2 kW/m <sup>2</sup> and a pitch of 1.5. ...	32



Figure 5.5. Transitional average Nusselt number (top) and Colburn *j-factor* (bottom) plotted against Reynolds number for the single and three-tube set-up for a heat flux of 3 kW/m<sup>2</sup> and a pitch of 1.5... 33

Figure 5.6. Transitional average Nusselt number (top) and Colburn *j-factor* (bottom) plotted against Reynolds number for the single and three-tube set-up for a heat flux of 4 kW/m<sup>2</sup> and a pitch of 1.5... 34

Figure 5.7. Average Nusselt number (top) and Colburn *j-factor* (bottom) plotted against Reynolds number for the single and three-tube set-up for a heat flux of 2 kW/m<sup>2</sup> and a pitch of 1.25. .... 35

Figure 5.8. Average Nusselt number (top) and Colburn *j-factor* (bottom) plotted against Reynolds number for the single and three-tube set-up for a heat flux of 3 kW/m<sup>2</sup> and a pitch of 1.25. .... 36

Figure 5.9. Average Nusselt number (top) and Colburn *j-factor* (bottom) plotted against Reynolds number for the single and three-tube set-up for a heat flux of 4 kW/m<sup>2</sup> and a pitch of 1.25. .... 37

Figure 5.10. Transitional average Nusselt number (top) and Colburn *j-factor* (bottom) plotted against Reynolds number for the single and three-tube set-up for a heat flux of 2 kW/m<sup>2</sup> and a pitch of 1.25. 38

Figure 5.11. Transitional average Nusselt number (top) and Colburn *j-factor* (bottom) plotted against Reynolds number for the single and three-tube set-up for a heat flux of 3 kW/m<sup>2</sup> and a pitch of 1.25. 39

Figure 5.12. Transitional average Nusselt number (top) and Colburn *j-factor* (bottom) plotted against Reynolds number for the single and three-tube set-up for a heat flux of 4kW/m<sup>2</sup> and a pitch of 1.25. . 40

Table 2.1. Nusselt number correlations for laminar and turbulent flow..... 11

Table 2.2. Range of Reynolds numbers for transitional flow for various inlet geometries ..... 12

Table 2.3. Coefficients for equation 2-13..... 12

Table 3.1. The specified range and calculated uncertainties for the instruments and tube. .... 21

Table 3.2. Uncertainties for the thermophysical properties of water in the range 0-150°C..... 22

Table 5.1. Critical Reynolds numbers (start of the transitional regime) for the left, centre and right tubes at varying pitches and heat fluxes. .... 41

Table 5.2. Transitional regime gradient for the left, centre and right tubes at varying pitches and heat fluxes. .... 41



## NOMENCLATURE

Symbol	Description	Units	Variations
$A$	Area	$m^2$	$A_c$ Cross-sectional area $A_s$ Surface area
$c_p$	Specific heat at constant pressure	$kJ/kg \cdot K$	
$D$	Diameter	$m$	$D_i$ Inner diameter $D_o$ Outer diameter
$g$	Gravitational acceleration	$m/s^2$	
$Gr$	Grashof number	-	$Gr_f$ Grashof number at $T_f$
$h$	Average heat transfer coefficient	$W/m^2 \cdot K$	$h_x$ Heat transfer coefficient at $x$
$k$	Thermal conductivity	$W/m \cdot K$	$k_w$ Tube wall thermal conductivity $k_b$ Fluid thermal conductivity at $T_b$
$L$	Length	$m$	$L_h$ Hydrodynamic entry length $L_t$ Thermal entry length
$\dot{m}$	Mass flow rate	$kg/s$	
$Nu$	Average Nusselt number	-	$Nu_x$ Nusselt number at $x$ $Nu_l$ Laminar Nusselt number $Nu_t$ Turbulent Nusselt number
$Pr$	Prandtl number	-	$Pr_f$ Prandtl number at $T_f$
$\dot{Q}$	Heat transfer rate	$W$	
$\dot{q}$	Heat flux	$W/m^2$	$\dot{q}_s$ Surface heat flux
$R$	Radius	$m$	
$Ra$	Rayleigh number	-	
$Re$	Reynolds number	-	$Re_{cr}$ Critical Reynolds number
$T$	Temperature	$^{\circ}C$	$T_i$ Inlet temperature $T_o$ Outlet temperature $T_{inner}$ Inner wall temperature $T_{outer}$ Outer wall temperature $T_b$ Bulk fluid temperature $T_f = (T_{inner} + T_b)/2$ $\bar{T}$ Average temperature
$t$	Tube wall thickness	$m$	
$V$	Velocity	$m/s$	$\bar{V}$ Average velocity
$\beta$	Volume expansivity	$1/K$	
$\mu$	Dynamic viscosity	$kg/m \cdot s$	$\mu_b$ Viscosity at bulk fluid temperature $\mu_w$ Viscosity at inner wall temperature
$\nu$	Kinematic viscosity	$m^2/s$	
$\rho$	Density	$kg/m^3$	



# 1. INTRODUCTION

## 1.1 BACKGROUND

The world's population is predicted to reach more than 9 billion people within the next 40 years (UNPF, 2015). This increase in population coupled with dramatically increasing urbanisation in developing countries imposes severe strain on the world's already limited resources. One such resource is energy in the form of electricity, with many developing and even developed countries battling to meet the population's electricity demand.

The world has only a finite amount of non-renewable resources like coal and natural gas and as these resources are depleted, the price to produce heat for the generation of electricity constantly increases. This has become a problem, especially in developing countries where a large percentage of the population is unable to afford what has become a basic human right, not to mention the implications these fossil fuels have on the environment. With as much as 75% of all electricity generation occurring in plants that use fossil fuels (Enerdata, 2015), there is a desperate need for an alternative means of electricity generation – one that is not only less expensive but also more sustainable.

Renewable resources such as wind and hydro-power are already being harnessed to produce electricity, but these resources require specific environments and conditions to be viable alternatives to traditional fossil fuel powered stations. Solar energy, on the other hand, is the most abundant source of energy on the planet and already many countries are harnessing this energy for the generation of electricity – either through photovoltaic collectors or through thermal systems such as concentrated solar power (CSP) systems (Perez, 2013).

CSP systems operate using mirrors which concentrate solar radiation and focus it onto a heat transfer surface, which is often the outer surface of a tube in the case of a trough system. The fluid inside this tube reaches temperatures of up to 400°C and is used to boil water to generate steam which can be used in a conventional generator to generate electricity. CSP systems, when used to generate heat on a commercial scale, require large areas of land for solar radiation collection. Since CSP technology is relatively new, it is important for designers of such systems to fully understand the heat transfer coefficients between the wall of the tube and the fluid flowing inside it to reduce the total size of the solar collection area. This would improve the efficiency and reduce the cost of building the system.

Heat transfer in heat exchangers can take place as either a uniform heat flux or as a constant wall temperature at the boundary of the tube. The former being the practical case of heating via electrical resistance and the latter being the case of heating via condensation/evaporation of another fluid on the outside of the tube. In both cases the heat transfer mechanism is convection, which is influenced by the flow regime (laminar, transitional or turbulent).

The non-dimensional Nusselt number, which describes the heat transfer coefficient, varies along the developing region of flow inside the tube. It also varies for each flow regime. The Nusselt number for fully developed flow in the laminar flow regime has been found, through experimental analysis, to be a constant. The value of this parameter is 4.36 for the uniform heat flux boundary condition, and 3.66 for the constant wall temperature boundary condition. Nusselt number correlations for turbulent flow are far more complex, as they are a function of friction factor, Reynolds number and Prandtl number. Several published articles present different formulae for calculating the Nusselt number in the turbulent flow regime, however each correlation yields a different solution. This can be attributed to the varying degrees of simplifications used and assumptions made. Perhaps the simplest correlation would be that of Dittus and Boelter (1930), but this can give rise to errors as high as 25 percent. For

conservative results, it is recommended that Gnielinski's equation (1976) be used (Çengel and Ghajar, 2014).

It is general practice to design heat exchangers to operate in the turbulent flow regime, since formulae are well established and the regime offers the best heat transfer characteristics. The negative aspect of this regime is the increased friction factor which results in a greater pressure drop between the inlet and the outlet of the tube – requiring a more powerful pump to drive the fluid. Fluid flowing in the laminar regime exhibits a much smaller pressure drop, but also far inferior heat transfer characteristics. Flow is said to be laminar for Reynolds numbers up to 2300 for circular tubes, and turbulent for Reynolds numbers of 4000 or more. However, this range is highly dependent on the specific conditions in the tube, such as inlet profile and tube roughness. The optimum design for a heat exchanger would thus be one in which both high heat transfer characteristics and low pressure drops are experienced. The desire for more efficient systems has thus driven researchers into conducting experiments that identify the specific relations for heat transfer and pressure drop for flow in the transitional flow regime.

Notable contributions to research in the transitional flow regime have been made by A.J. Ghajar at the Oklahoma State University and by J.P. Meyer at the University of Pretoria. In a study conducted by Ghajar and Tam (2013), the effects of different inlet geometries and heating on the friction factor in the entrance and fully developed regions of a horizontal tube for a range of Reynolds numbers was investigated using an ethylene glycol and water mixture. To cover the laminar, transitional and turbulent flow regimes, the Reynolds number ranged from 800 to 22 000. It was found that the constant heat flux boundary condition lowered the friction factor in the entrance and fully developed regions for both the laminar and transitional flow regimes. Correlations were developed for the prediction of non-isothermal entrance and fully developed friction factors for square-edged and re-entrant entrance profiles.

In another study by Ghajar and Tam (1994), an attempt to create a database for heat transfer correlations across the laminar, transitional and turbulent flow regimes for the square-edged, re-entrant and bellmouth inlet profiles was made. The experiment involved a horizontal tube subjected to a constant heat flux boundary condition. The study was successful in identifying the inlet profile dependence of the transitional flow regime Reynolds number range. It was also identified that the establishment of secondary flow was inlet profile dependent. Correlations were developed for predicting the heat transfer coefficients in both the entrance and fully developed regions for forced and mixed convection in all three flow regimes.

In a similar study by Meyer and Olivier (2013), the effect of inlet profile geometry on the heat transfer characteristics and pressure drop in the transitional flow regime was investigated. However, this study focused on the cooling of water inside the tube using a constant wall temperature boundary condition. It was identified that the transitional flow regime Reynolds number range was inlet profile dependent. Because of secondary flow, the diabatic friction factors were found to be inlet profile independent.

The investigations conducted by these researchers have laid the foundation for further investigation into the heat transfer characteristics of flow in the transitional flow regime. The database that has been started is, however, far from complete and further research is required to provide a complete understanding of this flow regime and to possibly allow the implementation of the new-found heat transfer correlations into the design handbooks of future engineers.



## 1.2 PROBLEM STATEMENT

Extensive research has been conducted on the heat transfer characteristics of flow in the transitional flow regime, as well as the effect of tube roughness, inlet profile geometries and heating boundary conditions. However, no research has been conducted on the effect that tube pitch ratios of a multiple tube inlet condition has on these characteristics.

## 1.3 OBJECTIVES

The aim of this investigation is to determine the effect of a multiple tube inlet condition on the heat transfer characteristics of flow in the transitional flow regime, including the design of the experimental facility. Measurements will be taken for pitch ratios of 1.25 and 1.5 on a three-tube heat exchanger to determine the heat transfer characteristics for a uniform heat flux boundary condition of 2, 3 and 4 kW/m<sup>2</sup>. The experiment is to be conducted on a smooth horizontal tube.

## 1.4 SCOPE OF WORK

This study was limited to experiments using water as a working fluid for two tube pitch ratios. It was furthermore limited to only a constant heat flux boundary condition and only fully developed flow was investigated.

## 1.5 CONTENT OF REPORT

This dissertation consists of a total of six chapters. In the following chapter (Chapter 2), the literature relevant to the topic of heat transfer in the transitional flow regime is discussed. Chapter 3 covers the experimental design, calculations and set-up, including the method of data capture and the heat transfer correlations used. The results obtained from the experimental set-up for the case of the validation tube and multiple tube set up are discussed and displayed graphically in Chapter 4 and Chapter 5 respectively. Finally, conclusions and recommendations are presented in Chapter 6.

## 2. LITERATURE STUDY

### 2.1 INTRODUCTION

The design of a heat exchanger requires a proper understanding of the aspects of fluid flow and heat transfer. This literature study discusses the fundamentals of these aspects as well as provides insight into the multiple tube inlet condition. Previous work which can be related to this investigation, as well as the shortcomings thereof, is discussed at the end of the chapter.

### 2.2 NON-DIMENSIONAL PARAMETERS

The scientific study of fluid flow inside tubes dates as far back as 1738 when Bernoulli (1738) published his work in his book entitled *Hydrodynamica*. Since then extensive research has been done on fluid flow inside tubes which has led to the establishment of several non-dimensional parameters which can be used to simplify the analysis of fluid flow.

#### 2.2.1 Reynolds number

Introduced by Stokes (1851) and popularised more than 30 years later by Reynolds (1883), the Reynolds number is a dimensionless quantity used to predict flow patterns in various applications. It is defined as the ratio of inertia forces to viscous forces and is calculated for circular pipes using equation 2-1 (White, 2003),

$$Re = \frac{\rho \bar{V} D}{\mu} = \frac{4\dot{m}}{\mu \pi D} \quad 2-1$$

#### 2.2.2 Nusselt number

In 1915, Wilhelm Nusselt (1915) published a paper in which he had formed several dimensionless groups. One of these parameters, termed the Nusselt number, was used to non-dimensionalise the heat transfer coefficient and is given in equation 2-2 (Çengel and Ghajar, 2014),

$$Nu = \frac{hD}{k} \quad 2-2$$

#### 2.2.3 Prandtl number

A dimensionless term named after Ludwig Prandtl (1875-1953) for his work on fluid boundary layers describes the relative thickness of the velocity and the thermal boundary layers as the ratio of molecular diffusivity of momentum to the molecular diffusivity of heat, expressed as equation 2-3 (Çengel and Ghajar, 2014),

$$Pr = \frac{\mu c_p}{k} \quad 2-3$$

#### 2.2.4 Grashof number

Named after Franz Grashof (1826-1893), the Grashof number is a non-dimensional parameter that represents the natural convection effects. It is essentially the ratio of buoyancy forces to viscous forces (Çengel and Ghajar, 2014) and is calculated using equation 2-4,

$$Gr = \frac{g\beta(T_i - T_b)D^3}{\nu^2} \quad 2-4$$

### 2.2.5 Rayleigh number

The non-dimensional parameter named after Nobel Prize Winner Lord Rayleigh (1842-1919) is described as the ratio of buoyancy forces and the product of thermal and momentum diffusivities. It is essentially the product of the Grashof and Prandtl numbers and is given as equation 2-5 (Çengel and Ghajar, 2014),

$$Ra = Gr \cdot Pr \quad 2-5$$

## 2.3 CLASSIFICATION OF FLUID FLOW

The classification of fluid flow as laminar, turbulent or transitional was introduced by Osborne Reynolds (1883). The easiest way to visualise the concept is to inject a stream of dye into a tube with flowing fluid and observe the stream as shown in Figure 2.1.

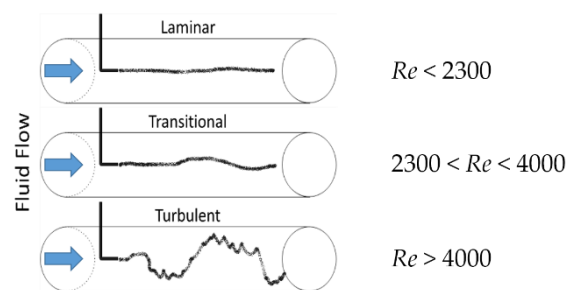


Figure 2.1. Injection of dye into a stream to visualise flow regimes.

Flow is said to be laminar when the stream is smooth and usually occurs for slower velocities. Flow becomes turbulent when the stream flows faster and becomes chaotic because of vortices and eddies. The transitional regime is the region where flow is not fully turbulent and still exhibits aspects of laminar flow. The classification of fluid flow in a smooth circular cross-section tube can be determined using the dimensionless Reynolds number also shown in Figure 2.1.

### 2.3.1 Factors influencing the flow regime

The transitional regime is difficult to predict and is not bounded to the ranges shown in Figure 2.1. Certain factors (apart from fluid velocity) can influence the onset of transition, such as tube roughness and inlet geometry. The regime can start at a Reynolds number as low as 2 000 for rough tubes with rough inlets or it can be delayed to a Reynolds number as high as 40 000 for smooth tubes with smooth inlets (Fung, 1990).

When the tube is heated to temperatures close to that of the critical point of the working fluid, or when there is a large difference between wall and mean bulk temperatures, the physical properties of the fluid itself can influence the onset of transition. This is attributed to the degradation of viscosity at critical points. Pipe vibrations from external sources or small fluctuations in fluid velocity may also trigger the onset of transition (Çengel and Ghajar, 2014).

## 2.4 THE ENTRANCE REGION

Consider a large tank of fluid being drained from a small tube attached to the bottom. As the fluid enters the tube, certain factors influence the length of tube required before the flow reaches a state of being fully developed. The different types of inlet geometries influence entry length.

### 2.4.1 Hydrodynamic entrance region

If the fluid enters the tube at uniform velocity, because of the no slip condition at the walls of the tube the fluid particles at the outer boundary do not move. Due to friction between particles, this layer of stationary particles slows the next layer of particles. To balance this friction effect and satisfy the continuity condition, the particles in the mid-section of the tube speed up.

The velocity boundary layer is the region where the viscous shearing effects are significant. This boundary layer divides the flow into the boundary layer region and the irrotational core region as shown in Figure 2.2. The boundary layer continues to grow until it reaches the tube centre, and shortly after the velocity profile is said to be fully developed. Fully developed velocity profiles are parabolic in shape for laminar flow, and the profile becomes more rounded for turbulent flow (Çengel and Ghajar, 2014).

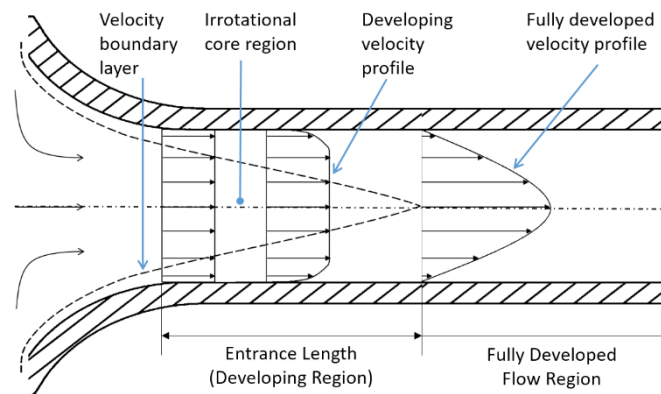


Figure 2.2. The hydrodynamic entry length.

### 2.4.2 Thermal entrance region

If the fluid inside the tube was at a constant temperature and the wall of the tube were to be held at a higher temperature, the fluid particles closest to the wall of the tube would be heated to the temperature of the tube wall. Through convection, the particles closer to the mid-section of the tube would also increase in temperature. This results in a thermal boundary layer similar to that of the velocity boundary layer and is shown in Figure 2.3. Flow is said to be fully developed when the velocity and temperature profiles remain unchanged (Çengel and Ghajar, 2014).

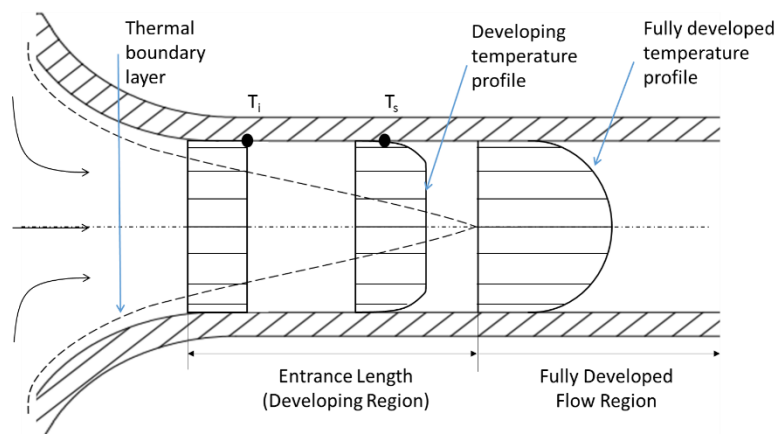


Figure 2.3. The thermal entry length.

### 2.4.3 Entry lengths

For fluids with a Prandtl number close to unity, the hydrodynamic and thermal entry lengths are essentially equal. However, for fluids with Prandtl numbers larger than unity, the thermal entry length outgrows the hydrodynamic entry length, with the opposite true for Prandtl numbers less than unity. Entry lengths differ for forced laminar and turbulent flow as follows (Çengel and Ghajar, 2014),

Laminar	Hydrodynamic	$L_h \approx 0.05 \cdot Re \cdot D$	2-6
	Thermal	$L_t \approx 0.05 \cdot Re \cdot D \cdot Pr$	2-7
Turbulent	Hydrodynamic/Thermal	$L_h = L_t \approx 10D$	2-8

It is important to know where in the tube the flow is fully developed since many equations and theories are only applicable to fully developed flow. Depending on the application and the expected results, it is sometimes necessary to allow the fluid to develop hydrodynamically before the tube is heated so that the necessary equations are applicable.

### 2.4.4 Types of inlets

The inlet geometry affects the fluctuations in flow velocity, which influences the heat transfer coefficient. This can promote or delay the onset of transition and turbulence. The four most common inlet geometries are given in Figure 2.4.

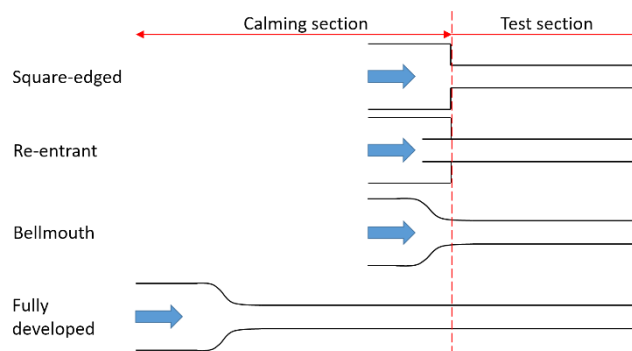


Figure 2.4. The four inlet geometries.

Square-edged and re-entrant geometries simulate the sudden contraction of tubes typically found in shell and tube heat exchangers, with the re-entrant geometry providing an extension of the tube into the header section promoting the onset of transition (Ghajar and Tam, 1997). The bellmouth geometry is not common in industry since the inlet is difficult to manufacture, however it does delay the onset of transition. The fully developed inlet is equivalent to the bellmouth except for the fact that the test section begins a distance from the inlet where flow has become fully developed.

## 2.5 FUNDAMENTALS OF HEAT TRANSFER

It is important to understand the fundamentals of heat transfer that can be applied to a heat exchanger set-up, such as the appropriate boundary conditions and heat transfer mechanisms within the flow.

### 2.5.1 Boundary conditions

The method in which heat is applied to the tubes of a heat exchanger is important to consider, since the variation in surface and fluid temperature along the length of the tube will differ in each case.

### 2.5.1.1 Uniform heat flux

The case of uniform heat flux at the boundary of the tube is the practical application of electric resistance heating. The result is a linearly increasing fluid temperature along the length of the tube. Once the flow is thermally fully developed, then the wall temperature also increases linearly as shown in Figure 2.5.

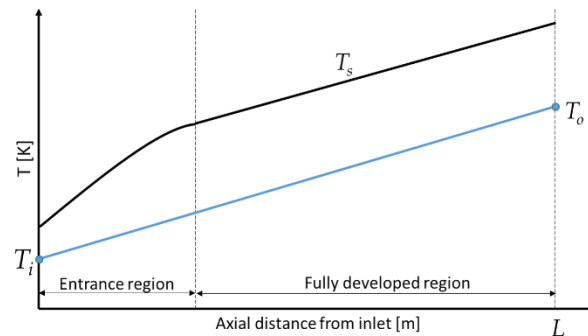


Figure 2.5. Surface ( $T_s$ ), inlet ( $T_i$ ) and outlet ( $T_o$ ) fluid temperature for the uniform heat flux boundary condition.

For this boundary condition in the fully developed flow region, the temperature gradient is independent of the axial position ( $x$ ) along the length of the tube and thus the shape of the temperature profile does not change in the axial direction (Çengel and Ghajar, 2014), as shown in equation 2-9,

$$\frac{\partial T}{\partial x} = \frac{2\pi R \cdot \dot{q}_s}{\dot{m}c_p} = \text{constant} \quad 2-9$$

### 2.5.1.2 Constant wall temperature

The case of the constant wall temperature at the boundary of the tube is the practical application of a fluid isothermally condensing/evaporating along the length of the tube. The tube wall temperature remains approximately constant, and depending on the length of the tube, the fluid velocity and fluid properties, the fluid temperature may approach the wall temperature but will never exceed it (in the case of heating) as shown in Figure 2.6.

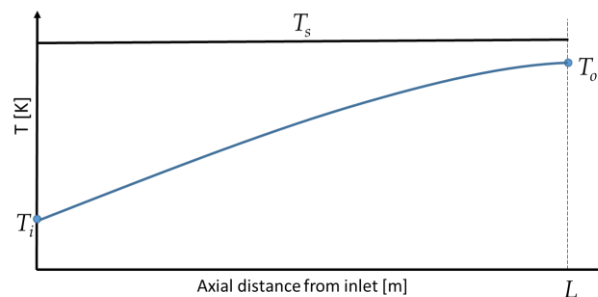


Figure 2.6. Surface ( $T_s$ ), inlet ( $T_i$ ) and outlet ( $T_o$ ) fluid temperature for the constant wall temperature boundary condition.

To describe the heat transfer between the fluid and the surface, the average temperature difference is required. This average value can accurately be represented by the logarithmic mean temperature difference (equation 2-10) instead of the arithmetic mean difference in an attempt to reduce approximation errors (Çengel and Ghajar, 2014),

$$\Delta T_{lm} = \frac{(T_s - T_o) - (T_s - T_i)}{\ln\left(\frac{T_s - T_o}{T_s - T_i}\right)} = \frac{\Delta T_o - \Delta T_i}{\ln\left(\frac{\Delta T_o}{\Delta T_i}\right)} \quad 2-10$$

## 2.5.2 Forms of heat transfer

Neglecting radiation effects, heat is transferred via conduction and convection (forced and natural) in the tubes of heat exchangers. Conduction is the mechanism whereby heat is transferred between neighbouring particles, with the requirement being that the two particles are in contact. The rate at which heat is transferred by conduction is given by Fourier's law in equation 2-11,

$$\dot{Q}_{cond} = kA_c \frac{\Delta T}{\Delta x} \quad 2-11$$

Convection is the mechanism whereby heat is transferred between a solid surface and fluid in motion passing over this surface. The heat transfer coefficient is dependent on factors such as flow velocity and is difficult to predict. The coefficient is thus often obtained from literature or from studies conducted in a similar environment. The rate at which heat is transferred by convection is given by Newton's law of cooling in equation 2-12,

$$\dot{Q}_{conv} = hA_s \Delta T \quad 2-12$$

Forced convection is described by the process of heating the tube, but a notable phenomenon experienced in heated tubes is the process of natural convection. As the tube is heated, the temperature of the fluid closest to the walls becomes hotter than the fluid in the centre. This results in a density distribution that is non-uniform and thus, because of gravity, the fluid in the centre of the tube begins to sink and the fluid at the outer edges begins to rise. The process is shown in Figure 2.7 and is termed secondary flow.

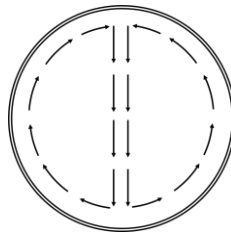


Figure 2.7. Secondary flow within the tube cross-section.

When the tube is heated via a uniform heat flux, secondary flow is experienced along the entire length of the tube. Whereas in the case of heating via constant wall temperature, as the fluid temperature approaches that of the tube wall, the density distribution along the cross-section becomes more uniform and thus the secondary flow diminishes. Natural convection tends to aid heat transfer in horizontal tubes as the secondary flow currents create a mixing effect and thus heat is dissipated faster.

The heat transfer coefficient for forced convection is usually several factors greater than that of natural convection and thus in practice it is usually acceptable to neglect the effects of secondary flow. Çengel and Ghajar (2014) however, present a condition for when natural convection terms become insignificant:

Natural convection dominant	$\frac{Gr}{Re^2} \gg 1$
Forced convection dominant	$\frac{Gr}{Re^2} \ll 1$
Mixed convection	$\frac{Gr}{Re^2} \approx 1$

## 2.6 SHELL-AND-TUBE HEAT EXCHANGERS

Shell-and-tube heat exchangers are non-mixing fluid to fluid heat exchangers as shown in Figure 2.8. Heat is transferred through a conductive barrier in the form of metal tubes. This type of heat exchanger is widely used due to the advantages it offers over other types of heat exchangers. A shell-and-tube heat exchanger can be designed and built in various configurations where factory floor space may be a limiting factor. The heat exchangers are also simple to maintain and several authors have published handbooks which simplify the design process.

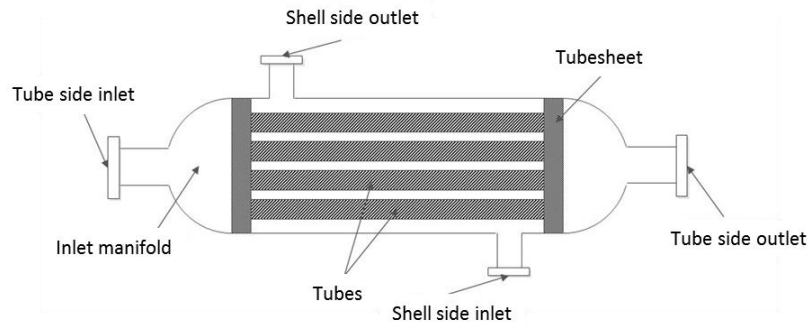


Figure 2.8. A simple shell-and-tube heat exchanger.

Since this study is focused on the effect of adjacent tubes at the tube side of the heat exchanger, the design of the shell side is not discussed. Design of the tube side involves tube size, pitch and configuration which all influence the pressure drop and heat transfer over the heat exchanger. A good design will ensure that the pressure drop is acceptably low whilst maintaining a high heat transfer coefficient. Byrne (2007) and the Tubular Exchanger Manufacturers Association (TEMA) present a best practice design methodology and standards for the optimal design of heat exchangers.

### 2.6.1 Tube configuration

Tubes inside the heat exchanger can be arranged in either a square or triangular configuration, or rotated variations thereof. Figure 2.9 shows the geometry of each configuration. Square configurations are typically used in applications where tube fouling is significant since this configuration is easier to clean. Triangular configurations are typically used in more compact heat exchangers where fouling is less likely to occur.

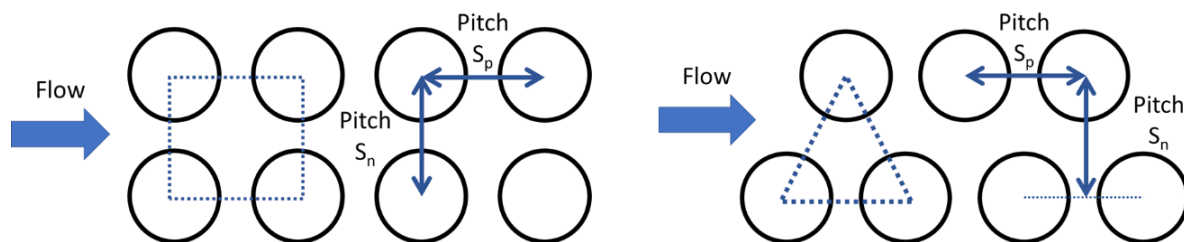


Figure 2.9. Shell-and-tube heat exchanger tube configuration – square (left) and triangular (right).

Tube diameters are selected using standard ASTM tube sizes, with  $\frac{3}{4}$ " and 1" being the most popular (Shah and Sekulic, 2003). The parallel and normal tube pitches,  $S_p$  and  $S_n$ , vary from 1.25 times the outer diameter of the tube to 3 times the outer diameter (Holman, 2010). However, designers rarely exceed a pitch of 1.5 since the overall size of the heat exchanger increases dramatically. Smaller pitches also tend to trip the flow in the shell side inducing turbulence and increasing overall heat transfer. To ensure that the tubesheet is sufficiently strong and that maintenance remains relatively simple, a minimum pitch of 1.25 is specified. Tube to tubesheet joints are made by either hydraulic or thermal expanding of the

tubes, rolling the tubes, or welding or brazing. This minimum pitch of 1.25 thus also ensures that these joints are easy to make and free from leaks.

### 2.6.2 Flow maldistribution

Fluid flow enters the tube side inlet and is distributed amongst the tubes. Design handbooks often assume that each tube receives equal mass flow. However, depending on the configuration of the inlet, this assumption is often incorrect. Depending on the inlet manifold design, the flow may be angled or off centre. Gotoda and Izumi (1978) found that irrespective of the inlet angle, the maximum velocity in any tube of the tube bundle never exceeded 1.2 times the mean tube velocity. However, they did note that the location in the tube with maximum velocity was dependent on inlet angle. Even if the flow enters the tube side at zero angle, uniform flow is almost never achieved. This maldistribution can impair thermal performance by as much as 10 percent.

## 2.7 PREVIOUS WORK

It is important to take note of the work done by previous researchers that relates to the topic of heat transfer in the transitional flow regime. The equations for Nusselt number are well established for flow in the laminar and turbulent flow regimes and particularly for fully developed laminar flow where the Nusselt numbers are constants: 4.36 for uniform heat flux boundary condition and 3.66 for the constant wall temperature boundary condition. Table 2.1 is an excerpt from Çengel and Ghajar (2014) and highlights some of the other well published Nusselt number correlations for flow in the laminar and turbulent flow regimes. A correlation by Morcos and Bergles (1975) is also included for laminar flow to account for secondary flow at higher heat fluxes.

Table 2.1. Nusselt number correlations for laminar and turbulent flow.

Author	Correlation	Regime	Condition
Petukhov (1969)	$Nu = 4.36 \left[ 1 + \left( \frac{Ra}{18000} \right)^4 \right]^{0.045}$	Laminar	
Morcos and Bergles (1975)	$Nu = \left\{ 4.36^2 + \left[ 0.055 \left( \frac{Gr_f Pr_f^{1.35}}{Pw^{0.25}} \right)^{0.4} \right]^2 \right\}^{0.5}$	Laminar	$3 \times 10^4 < Ra < 10^6$ $4 < Pr < 175$ $2 < Pw < 66$ $Pw = hD_i^2 / (k_w t)$
Edwards (1979)	$Nu = 3.66 + \frac{0.065 \cdot \frac{D}{L} \cdot Re \cdot Pr}{1 + 0.04 \left( \frac{D}{L} \cdot Re \cdot Pr \right)^{2/3}}$	Laminar	Entry region
Ghajar and Tam (1994)	$Nu_x = 1.24 \left[ \left( \frac{D \cdot Re \cdot Pr}{x} \right) + 0.025 (Gr \cdot Pr)^{0.75} \right]^{1/3} \left( \frac{\mu_b}{\mu_w} \right)^{0.14}$	Laminar	$280 \leq Re \leq 3800$ $40 \leq Pr \leq 160$ $3 \leq \frac{x}{D} \leq 192$ $1.2 \leq \frac{\mu_b}{\mu_s} \leq 3.8$
Dittus and Boelter (1930)	$Nu = 0.023 Re^{0.8} Pr^n$	Turbulent	$1000 \leq Gr \leq 28000$ $2500 \leq Re \leq 124000$ $0.7 \leq Pr \leq 120$ $n = 0.4$ (heating) $n = 0.3$ (cooling)
Gnielinski (1976)	$Nu = \frac{\left( \frac{f}{8} \right)^{-2} (Re - 1000) Pr}{1 + 12.7 \left( \frac{f}{8} \right)^{0.5} (Pr^{2/3} - 1)}$	Turbulent	$3000 \leq Re \leq 5 \cdot 10^6$ $0.5 \leq Pr \leq 2000$ Fully developed $f = 0.79 \ln(Re) - 1.64$
Ghajar and Tam (1994)	$Nu_x = 0.023 Re^{0.8} Pr^{0.385} \left( \frac{x}{D} \right)^{-0.0054} \left( \frac{\mu_b}{\mu_w} \right)^{0.14}$	Turbulent	$7000 \leq Re \leq 49000$ $4 \leq Pr \leq 34$ $3 \leq \frac{x}{D} \leq 192$ $1.1 \leq \frac{\mu_b}{\mu_s} \leq 1.7$

### 2.7.1 Work of Ghajar

The Nusselt number correlations for flow in the transitional flow regime have been thought to lie between the values experiences in the laminar and turbulent flow regimes, since transitional flow exhibits flow characteristics of both regimes. Ghajar and his associates experimented with the influence different inlet geometries had on the heat transfer characteristics of flow in the transitional regime. Their experiment showed that the onset of transition was greatly affected by the inlet profile, and the range of Reynolds numbers where transitional flow was experienced is shown in Table 2.2 (Ghajar and Tam, 1994).

Table 2.2. Range of Reynolds numbers for transitional flow for various inlet geometries

<i>Inlet profile</i>	<i>Transition range</i>
Square-edged	2 400 < Re < 7 300
Re-entrant	2 000 < Re < 6 700
Bellmouth	3 400 < Re < 9 400

Ghajar and Tam (1994) developed a correlation for the heat transfer coefficient which is given in equation 2-13,

$$Nu_{tr} = \left[ Nu_l + e^{\frac{a-Re}{b}} + Nu_t^c \right]^c \quad 2-13$$

The coefficients a, b and c are inlet profile dependent and are given in Table 2.3 together with the conditions of validity.

Table 2.3. Coefficients for equation 2-13.

<i>Square-edged</i>			<i>Re-entrant</i>			<i>Bellmouth</i>		
<i>a</i>	<i>b</i>	<i>c</i>	<i>a</i>	<i>b</i>	<i>c</i>	<i>a</i>	<i>b</i>	<i>c</i>
2617	207	-0.950	1766	276	-0.955	6628	237	-0.980
1 600 ≤ Re ≤ 10 700			1 700 ≤ Re ≤ 9 100			3 300 ≤ Re ≤ 11 100		
5 ≤ Pr ≤ 55			5 ≤ Pr ≤ 51			13 ≤ Pr ≤ 77		
3 ≤ $\frac{x}{D}$ ≤ 192			3 ≤ $\frac{x}{D}$ ≤ 192			3 ≤ $\frac{x}{D}$ ≤ 192		
1.2 ≤ $\frac{\mu_b}{\mu_w}$ ≤ 2.6			1.2 ≤ $\frac{\mu_b}{\mu_w}$ ≤ 2.2			1.2 ≤ $\frac{\mu_b}{\mu_w}$ ≤ 3.1		
4 000 ≤ Gr ≤ 25 000			4 000 ≤ Gr ≤ 21 000			6 000 ≤ Gr ≤ 11 000		

### 2.7.2 Work of Meyer

Meyer and his research team have also performed numerous studies on flow in the transitional flow regime. Where Ghajar and Tam (1994) used ethylene-glycol-water mixtures as a test fluid, Meyer has predominantly used water as a test fluid. In a particular study by Meyer and Olivier (2010), the aim was to investigate the effect of various inlet geometries of a test section being cooled at a constant wall temperature boundary condition. The experiment concluded that the onset of transition was not affected by the inlet profile and that transitional flow occurred for a Reynolds number range of 2 000 to 3 000. This result is in disagreement with that of Ghajar and Tam (1994), and was attributed to buoyancy induced secondary flow dampening the growth of the hydrodynamic boundary layer. Correlations were developed to predict the heat transfer coefficient in the laminar, turbulent and transitional flow regime. The correlation for the transitional regime is expressed in equation 2-14 and predicts the heat transfer coefficient to within 1%.

$$Nu_{tr} = \left[ Nu_l + e^{\frac{Re-2717}{202}} + Nu_t^{0.845} \right]^{-0.845} \quad 2-14$$



### 2.7.3 Shortcomings of previous work

Extensive research has been conducted by both Meyer and Ghajar. The effects of inlet profile geometries have been investigated by both researchers. Ghajar has published correlations for predicting heat transfer in the transitional flow regime for ethyl-glycol-water mixtures under a uniform heat flux boundary condition and Meyer has published correlations suited to flow in the transitional flow regime to predict heat transfer coefficients for water under a constant wall temperature boundary condition.

Despite the success of these investigations, no research has been conducted into investigating the effects of a multiple tube inlet condition on heat transfer in the transitional flow regime.

## 2.8 CONCLUSION

In conclusion, this chapter has discussed the non-dimensional parameters used in the literature to describe and predict heat transfer phenomenon. The classification of fluid flow has been established with the details regarding effective Reynolds numbers range of each regime. The various inlet geometries and their effects on fluid flow have been identified. Methods for calculating entry lengths have been discussed, and a brief overview of shell-and-tube heat exchangers is given. A short discussion of previous work in the field of transitional flow has been presented. The literature study concludes that although extensive research has been conducted on transitional flow, the effect of multiple tubes on heat transfer is unknown. The literature study has laid the foundation for the rest of the investigation.

### 3. EXPERIMENTAL SET-UP

#### 3.1 INTRODUCTION

This chapter serves to describe the experimental set up used in acquiring the data for this investigation into determining the effect of the multiple tube inlet condition on heat transfer. An overview of the instrumentation and equipment used in this experiment is given after which the method of data capture and data reduction is discussed. The result of the uncertainty analysis is also given and discussed.

#### 3.2 EXPERIMENTAL SET-UP

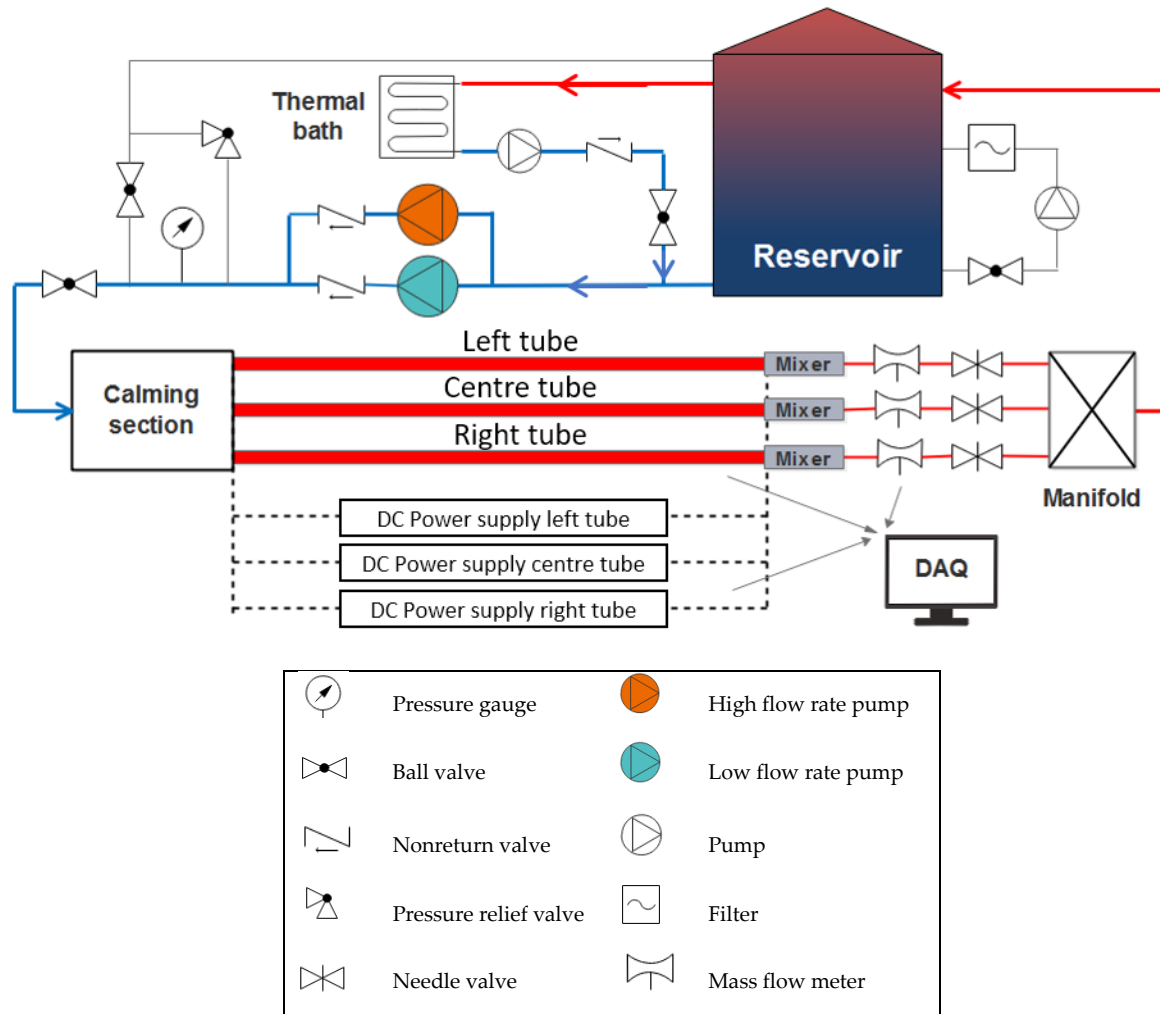


Figure 3.1. Schematic representation of the experimental set-up showing the multiple tube arrangement.

A schematic representation of the experimental set-up is given in Figure 3.1. The figure shows a closed loop system circulating water as the test fluid from a 280 litre reservoir through the multiple tube test section. Using a calibrated T-type thermocouple for ambient temperature reference, the reservoir is maintained at a constant temperature equal to the room temperature of the air-conditioned laboratory (22°C) using a Lauda thermal bath with a maximum cooling capacity of 900 W. This ensured no heat transfer occurred between the laboratory and the test fluid over the length of the supply line to the calming section. A filtration system constantly circulates the water in the reservoir to remove any algae or macro contaminants in the flow loop.

Two electronically variable speed pumps in parallel are used to provide the required pressure and flow rate: a low flow rate positive displacement pump used for lower Reynolds numbers and a high flow rate centrifugal pump used for higher turbulent Reynolds numbers. Nonreturn valves are installed at the outlet of both pumps to ensure that either pump can be individually selected without the need to manually open and close valves.

A bypass line is installed with a ball valve allowing some flow to return to the reservoir while the remainder is circulated in the test section. Another ball valve is installed on the supply line to the calming section. This allows the pumps to be run at higher backpressures and higher speeds reducing mass flow fluctuations. The 10-meter supply line to the calming section manufactured of flexible hose further reduces flow fluctuations by dampening out pulses and vibrations.

A pressure relief valve was installed as a safety precaution and a pressure gauge was used to monitor the pressure within the test section at any moment. These safety precautions ensure that the calming section was never over-pressurized and prevent the possibility of it rupturing. Needle valves were installed at the outlet of the mass flow sensors which were used to choke the flow and equalize the flow rate in each tube.

### 3.3 CALMING SECTION

A calming section was built using the design guidelines given by Ghajar and Tam (1994) and is shown in Figure 3.2. The scale given in the literature was enlarged by a factor of 1.4 to match the minimum recommended contraction ratio of 11:1 for the case of multiple tubes. The contraction ratio for the case of the single tube however is much larger at 58:1.

Following the design recommendation produced a 232 mm inner diameter PVC tube, 1.1 meters in length. 3D printed screens with an open-air ratio of 0.31 and stainless-steel meshes with an open-air ratio of 0.92 were installed to create a uniform flow distribution. Plastic soda straws were tightly packed and installed between the stainless-steel meshes to straighten the flow. An Omega PT100 temperature probe was installed at the inlet of the calming section to measure the bulk fluid inlet temperature. The probe was located far from the inlet of the test section and any effects on maldistribution are dampened out over the length of the calming section. The result was a uniform flow distribution at the inlet of the test section.

A simple inexpensive mechanical seal was designed to seal the test section against the end cap without the need for standard fittings. This ensured that the three tubes could be spaced close enough together to achieve the desired pitch spacing. Gasket maker was applied to the outer circumference of the tube and allowed to dry before compressing it against the end cap using bolts.

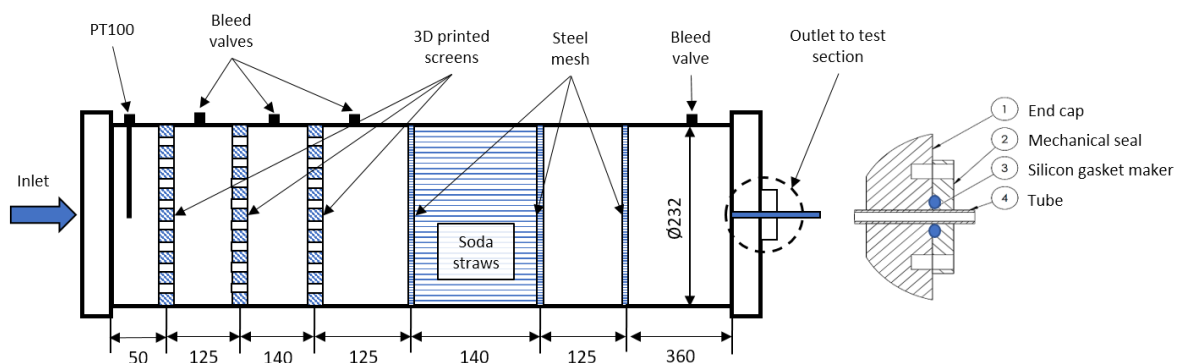


Figure 3.2. Cross-sectional view of the calming section showing screen inserts and the mechanical seal. Dimensions in [mm].

Bleed valves were installed to bleed air when priming the calming section. The bleed hole closest to the test section was used to ensure a square-edged inlet condition by inserting a boroscope into the hole and adjusting the tubes as required.

### 3.4 TEST SECTION

The single-tube validation test section as well as the three-tube test section were manufactured using 4mm inner diameter 316L stainless-steel tubes with a wall thickness of 1mm. The tubes were measured to be 6 meters in length and the tolerance on the outer diameter and wall thickness is given as  $\pm 0.038$  mm by the manufacturer. The tubes were insulated with 150 mm thick insulating foam with a thermal conductivity of 0.034 W/mK resulting in a heat loss of less than 3% at worst case conditions.

The test section was heated by passing current through the test section itself. The stainless-steel tubes were calculated to have an electrical resistance of  $0.282 \Omega$  at  $20^\circ\text{C}$ . This resistance value was used to calculate approximate current and voltage levels required for each heat flux before setting adjusting each of the three Elektro-Automatik PS 9040-60 DC power supplies. A computer interface program allowed the fine tuning of these current and voltage values by providing an accurate readout of the true input power to the test section.

As indicated in Figure 3.1, the tubes are assigned a naming convention – Left, Centre and Right with the Left tube being the first tube from the left when observing the test section from the calming section following the direction of flow.

Omega T-type thermocouples with a limit of error of  $0.1^\circ\text{C}$  were used to measure the outer surface temperature of the test section. The thermocouples were glued into 0.5mm holes, drilled 0.5mm deep spaced  $90^\circ$  apart as indicated in Figure 3.3. Arctic Alumina adhesive with a thermal conductivity of 9 W/mK was used to attach the thermocouples. Thirteen thermocouple stations comprising of three thermocouples each were used to find the average wall temperature of the test section at select axial locations as shown in Figure 3.4. The table in Figure 3.3 indicates the alternating manner in which thermocouples B and D were attached. This was done due to spatial limitations between the adjacent tubes' outer surfaces.

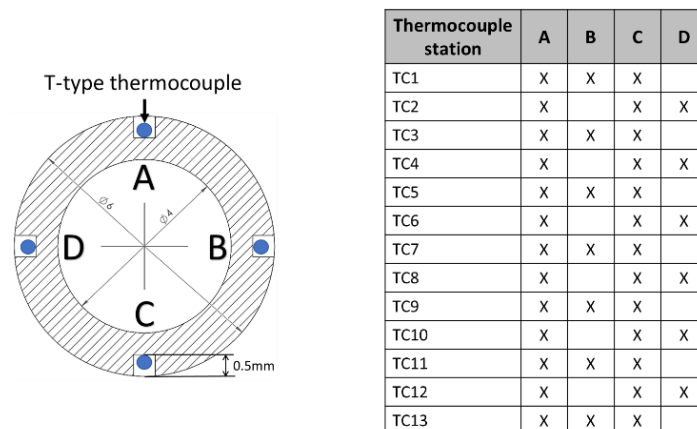


Figure 3.3. Cross-sectional view of the tube showing thermocouple orientations (left) and the alternating manner in which thermocouples B and D were attached (right).

Meyer and Olivier (2010) discuss how the method of thermocouple attachment can change the properties of the thermocouple junction and thus an in-situ method for thermocouple calibration was used. Water was circulated from the thermal bath through the test section and the thermocouple readings were logged after waiting for steady state conditions. Inlet and outlet temperatures were

measured using calibrated PT100 probes and were used as a reference for calibration. A detailed description of the calibration process is given in Appendix A.

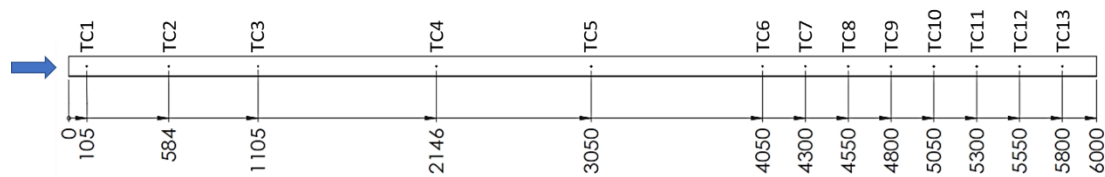


Figure 3.4. Axial locations of the thermocouple stations showing a concentration of stations in the fully developed region.

3D printed spacers were positioned along the length of the three-tube test section at approximately 0.5 m intervals which ensured the spacing between the tubes remained constant. Each tube was electrically insulated using a layer of Kapton tape which prevented the risk of electrical short circuits or sparks.

### 3.5 MIXING SECTION

To ensure the PT100 probe measured the uniform bulk outlet temperature of the test section, a mixer block as shown in Figure 3.5 was designed and built. The copper mixer plates were based on the design given by Bakker *et al.* (2000) and are used to effectively split the thermal boundary layer and promote mixing. Five plates 12 mm long and 8 mm wide each rotated 90° were soldered perpendicular to each other and inserted into the housing block upstream of the PT100 probe.

The housing block was manufactured using acetyl for its relatively low thermal conductivity and was insulated to the same specification as the test section. The design ensured the flow travelled over the full length of the PT100 probe greatly reducing flow stagnation in the mixer block and increasing the thermal response time of the system. A bleed valve was installed to occasionally bleed any air that passed through the test section and became trapped in the housing block.

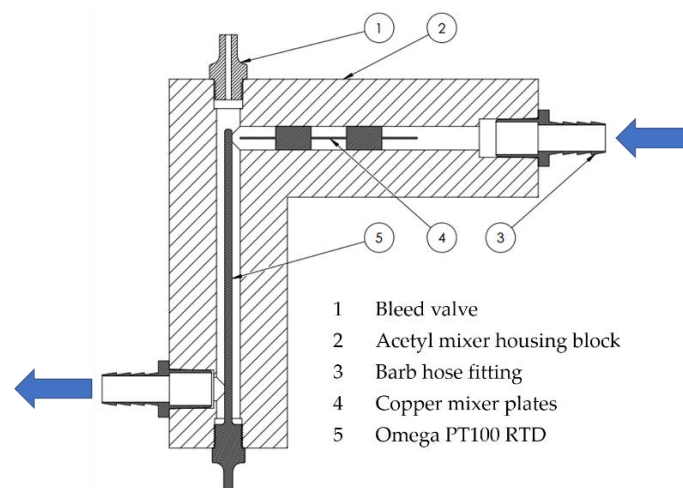


Figure 3.5. The mixer block designed to ensure accurate measurement of the fluid bulk outlet temperature.

#### 3.5.1 Manifold

A manifold consisting of three inlets downstream of each mixer block was used to combine the three flow streams from each tube and return the flow along a single line back to the reservoir. This ensured the outlet flow resistance of each tube was identical allowing equal distribution of flow in each of the three tubes.

## 3.6 INSTRUMENTATION

### 3.6.1 Power supply

Three identical Elektro-Automatik PS 9040-60 DC power supplies were used in the investigation, one for each tube. These power supplies were connected to the stainless-steel tubes using custom brass lugs that accommodated the close pitch spacing and allowed equal heating length on all three tubes.

Each power supply has a maximum power output of 1 500 W, a maximum voltage of 40 V and maximum current of 60 A. The manufacturer specifies the accuracy of the nominal voltage and current to be less than 0.2%. The power supplies were equipped with a 'sense' feature that measured the voltage drop over the length of the supply cable and compensated automatically giving a true reading of current and voltage over the length of the test section. As the test section heated up, the resistance of the tube increased. This was accounted for by monitoring the voltage and current readings during testing and adjusting as needed to maintain a constant heat flux over the tube.

### 3.6.2 Flow meters

Three identical Micro Motion CMF010 Coriolis flow meters were installed downstream of the mixing blocks to measure the mass flow in each tube. The manufacturer specifies the accuracy of the flow meter to be within 0.05% of the full-scale value of 1.36 kg/min. All three flow meters were calibrated by the manufacturer.

### 3.6.3 RTD probes

Four Omega PT100 RTD probes with an accuracy of 0.06°C were used to measure the bulk fluid temperature at the inlet and outlets of the test section. A single probe was placed in the calming section measuring the bulk inlet temperature of all three tubes, and the remaining three probes were inserted into the mixing blocks described in section 3.5 measuring the bulk outlet temperature of each tube individually. The probes were calibrated in the thermal bath using a Lauda DigiCal digital thermometer with an accuracy of 0.03°C as a reference.

### 3.6.4 Data acquisition

The data acquisition system used in this investigation was supplied by National Instruments. The SCXI-1001 chassis was fitted with a SCXI-1308 current input card for mass flow data capture, a SCXI-1306 resistive measurement card for PT100 data capture, a SCXI-1325 voltage terminal block for pump control and four SCXI-1303 32-channel thermocouple cards for outer wall temperature data capture.

This system was connected to a computer using LabView as the data logging software. The LabView interface was programmed to graphically display mass flow measurements, inlet and outlet temperature measurements and test section outer wall temperature measurements against time which were used to verify steady-state conditions had been reached before logging data. A MATLAB script was then used to process the raw data outputted by the LabView program.

## 3.7 DATA REDUCTION

To graphically display data and compare it to literature, the raw data outputted by the system needs to be converted to common units. This section explains the data reduction technique and formulae used in obtaining the quantities shown in Chapter 5.

### 3.7.1 Energy balance

As described in section 3.4, the energy input to the test section was calculated using the electrical resistance of the tubes and manipulating the current and voltage to achieve the desired input value.

$$\dot{Q}_{electric} = IV \quad 3-1$$

Equation 3-1 was used to determine the required voltage and current levels to be set on the power supplies to achieve the desired input power where  $I$  and  $V$  are the measured current and voltage drop of each tube. The total heat transferred to the test fluid was calculated using equation 3-2 where  $\dot{m}$  is the measured mass flow rate and  $T_o$  and  $T_i$  are the measured bulk outlet and inlet temperature. The specific heat property value  $C_p$  was interpolated from water property tables provided by Çengel and Ghajar (2014) at a bulk fluid temperature in the middle of the test section (equation 3-9).

$$\dot{Q}_{water} = \dot{m}C_p(T_o - T_i) \quad 3-2$$

The energy losses through the insulation material can thus be calculated using equation 3-3. The average energy lost over all measurements was found to be less than 3% with a maximum loss of 6% occurring at the lowest Reynolds number of 1 000 and at the highest heat flux of 4 kW/m<sup>2</sup>.

$$Energy\ lost\ [\%] = \left| \frac{\dot{Q}_{electric} - \dot{Q}_{water}}{\dot{Q}_{electric}} \right| \times 100 \quad 3-3$$

The heat flux applied to the test section is found using equation 3-4,

$$\dot{q} = \frac{\dot{Q}_{water}}{A_s} = \frac{\dot{Q}_{water}}{\pi D_i L} \quad 3-4$$

### 3.7.2 Temperature

The thermal resistance across the wall thickness of the tube was calculated using equation 3-5. However, since the thermocouples were attached into holes drilled 0.5 mm into the tube, an outer diameter of 5 mm instead was used instead of the tubes' outer diameter of 6 mm.

$$R_{tube} = \frac{\ln\left(\frac{D_o}{D_i}\right)}{2\pi k_w L} \quad 3-5$$

The temperature drop between the outer surface and the inner surface of the tube can be calculated using equation 3-6,

$$\Delta T = \dot{Q}R_{tube} \quad 3-6$$

The inner surface temperature at any thermocouple station can be found by subtracting the temperature drop found in equation 3-6 from the measured outer wall temperature, which was taken as the average of the thermocouples at a specific station:

$$T_{inner}(x) = T_{outer}(x) - \Delta T \quad 3-7$$

The average inner surface temperature of the test section in the fully developed test region was calculated using the trapezoidal rule to approximate the integral in equation 3-8,

$$\bar{T}_{inner} = \frac{1}{L} \int_0^L T_{inner}(x) dx \quad 3-8$$

The fluid temperature in the test section increased linearly as described in Figure 2.5. The mean fluid temperature at any location in the test section could thus be calculated using equation 3-9,

$$T_m(x) = \left(\frac{T_o - T_i}{L}\right)x + T_i \quad 3-9$$



The bulk fluid temperature was calculated using equation 3-9 at an  $x$ -location equal to 4.925 m corresponding to the middle of the fully developed test region.

### 3.7.3 Reynolds number

The Reynolds number was evaluated at the bulk fluid temperature using equation 3-10,

$$Re = \frac{4\dot{m}}{\mu_b \pi D_i} \quad 3-10$$

### 3.7.4 Heat transfer parameters

The average and local heat transfer coefficients can be calculated using equations 3-11 and 3-12 respectively,

$$h = \frac{\dot{q}}{\bar{T}_{inner} - T_b} \quad 3-11$$

$$h_x = \frac{\dot{q}}{T_{inner}(x) - T_m(x)} \quad 3-12$$

The average and local Nusselt numbers were calculated using equations 3-13 and 3-14 respectively,

$$Nu = \frac{hD_i}{k_b} \quad 3-13$$

$$Nu_x = \frac{h_x D_i}{k} \quad 3-14$$

where the thermal conductivity of the water was evaluated at the bulk temperature of the test section when calculating the average Nusselt number. The heat transfer results are displayed in terms of the Colburn  $j$ -factor to show the variation in Prandtl number, which was calculated using equation 3-15,

$$j = \frac{Nu}{RePr^{\frac{1}{3}}} \quad 3-15$$

## 3.8 EXPERIMENTAL PROCEDURE

Data were collected over a range of 1 000 to 7 000 Reynolds numbers ensuring all three flow regimes – namely the laminar, transitional and turbulent regimes – were adequately represented. Since the flow at a maximum Reynolds number of 7 000 proved to be fully turbulent and the focus of this study was on the transitional regime, it was deemed unnecessary to test at higher Reynolds number which would only induce higher pressures in the calming section.

The mass flow rate in the test section was controlled by setting the pumps to a high speed, and using the valves described in section 3.2 to achieve the desired Reynolds number. Fine adjustments in mass flow were performed by adjusting the voltage supply through the LabView interface. Meyer and Olivier (2010) demonstrated that the effects of hysteresis in the transitional regime were negligible, and thus experiments were conducted for decreasing flow rates only. This lessened the amount of time required between measurements for steady state conditions to be reached due to less residual heat stored in the insulation.

The heat flux applied to each tube was adjusted using the LabView power supply interface. The true input power, current and voltage were closely monitored and adjusted as the resistance of the tube changed.

Steady state conditions were monitored closely using live data plots for mass flow and temperature against time and data was only captured once these plots showed no visible gradient. The system took approximately 1 hour after start up to achieve steady state conditions where no changes in temperature, power or mass flow rates were observed for 10 minutes. The time between measuring points varied greatly through the different flow regimes – approximately 5 minutes in the laminar regime, 20 minutes in the transitional regime and 10 minutes in the turbulent regime.

Attention was given to data capture in the transitional regime, where data was logged for Reynolds number decrements of 50. In the laminar and turbulent regimes, the Reynolds number decrements were increased to 100 and 200 respectively. A live plot for calculated Reynolds number at any given moment in any of the three tubes was included in the LabView interface which allowed fine control over the Reynolds number decrements.

Once steady state conditions had been reached, a minimum of 200 data points were logged at a frequency of 10 Hz. The average of these data points was used to calculate the values described in section 3.7.

### 3.9 UNCERTAINTY

The method proposed by Dunn (2010) was used to calculate the uncertainties of the parameters described in the data reduction section within a 95% confidence interval. A linear regression analysis is used to find the uncertainties of the thermocouples and PT100 probes where the standard deviation of the sample points multiplied with Student's *t*-variable together with the manufacturer given accuracies are used to calculate the final uncertainty. The uncertainties for Nusselt number and Colburn *j*-factor can then be calculated using the method proposed by Dunn (2010).

#### 3.9.1 Equipment uncertainty

Table 3.1 highlights the range and accuracy of the instrumentation and the tube itself, considering the manufacturer specified accuracy together with the calculated uncertainty. The average uncertainty of all thermocouples is given as an indication. However, in calculation of the uncertainties of the Nusselt number and Colburn *j*-factor each thermocouple is individually assessed.

Table 3.1. The specified range and calculated uncertainties for the instruments and tube.

<i>Equipment</i>	<i>Range</i>	<i>Uncertainty</i>
Thermocouples	0 – 150 °C	±0.1 °C
Inlet PT100		±0.0606 °C
Outlet PT100 – Right tube		±0.0603 °C
Outlet PT100 – Centre tube	0 - 100 °C	±0.0606 °C
Outlet PT100 – Left tube		±0.0602 °C
Flow meters	0 - 81.6 kg/hour	±0.0408 kg/hour
Tube inner diameter & wall thickness	N/A	±0.038 mm
Tube length		±0.1 mm
Power supplies	0 – 40 V 0 – 60 A	±0.2% of nominal value

### 3.9.2 Fluid property uncertainty

Popiel and Wojtkowiak (1998) developed relations and list the uncertainties for the thermophysical properties of water in the range of 0-150°C. An excerpt from the article is given as Table 3.2. The article highlights the fact that the uncertainties in the transport properties of water (thermal conductivity, dynamic viscosity and Prandtl number) are significantly higher than the other properties which is shown below.

Table 3.2. Uncertainties for the thermophysical properties of water in the range 0-150°C.

Property	$\rho$	$\beta$	$c_p$	$k$	$\mu$	$Pr$
Uncertainty	0.004%	0.5%	0.06%	2.0%	1.0%	2.3%

### 3.9.3 Calculated uncertainties

Using the uncertainties found for the thermocouples and PT100 probes as well as the uncertainties in tube diameter and length together with the uncertainties for the properties of water, the overall uncertainty for Reynolds number, Nusselt number and Colburn j factor can be calculated. This section describes the method proposed by Dunn (2010) to calculate the uncertainties of these parameters.

#### 3.9.3.1 Reynolds number

Using the equation for Reynolds number (equation 3-10), the uncertainty can be calculated using equation 3-16. A sample calculation is provided in Appendix B.

$$\delta Re = \frac{4}{\pi} \left[ \left( \frac{1}{\mu_b D_i} \delta \dot{m} \right)^2 + \left( -\frac{\dot{m}}{\mu_b^2 D_i} \delta \mu_b \right)^2 + \left( -\frac{\dot{m}}{\mu_b D_i^2} \delta D_i \right)^2 \right]^{0.5} \quad 3-16$$

The uncertainties for Reynolds number are summarised graphically in Figure 3.6. From the figure, the Reynolds number uncertainty decreased for increasing Reynolds numbers. A sharp discontinuity is evident between 2 000 and 3 000 Reynolds number where the flow transitioned from laminar to turbulent. This increase in uncertainty is due to the increased standard deviation in mass flow rate caused by the instability of the transitional flow regime. In the fully turbulent regime, the uncertainty is constant at 1.4%. Over the entire regime, the uncertainty for Reynolds number does not exceed 1.8%.

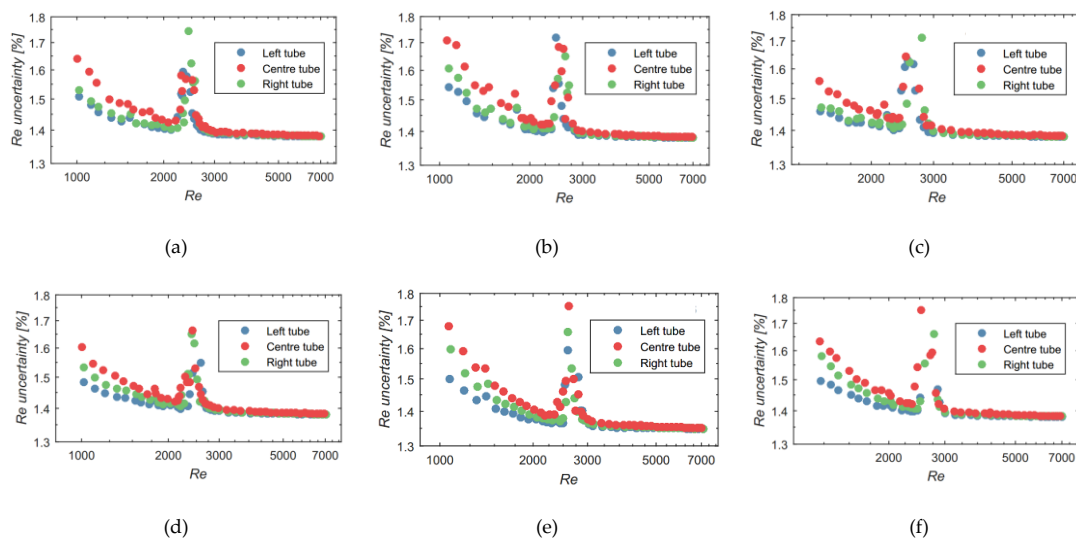


Figure 3.6. The uncertainty for Reynolds number at a pitch of 1.5 for 2, 3 and 4 kW/m<sup>2</sup> are given in (a), (b) and (c) respectively and the uncertainty at a pitch of 1.25 for 2, 3 and 4 kW/m<sup>2</sup> are given in (d), (e) and (f) respectively.

### 3.9.3.2 Temperature

The test section consisted of 13 thermocouple stations, and each station consisted of 3 thermocouples. The average temperature of all three thermocouples is used in calculating the heat transfer parameters, and thus the uncertainty of the average temperature at a station is calculated using equation 3-17. Note, due to the alternating thermocouples B and D described in Figure 3.3, either thermocouple B or D is used in the equation.

$$\delta \bar{T}_{inner} = \frac{1}{3} [(\delta T_A)^2 + (\delta T_{B/D})^2 + (\delta T_C)^2]^{0.5} \quad 3-17$$

### 3.9.3.3 Heat transfer area

The uncertainty of the effective heat transfer area is calculated using equation 3-18,

$$\delta A = \pi [(L\delta D_i)^2 + (D_i\delta L)^2]^{0.5} \quad 3-18$$

### 3.9.3.4 Heat input and heat flux

The uncertainties of the heat input and heat flux are calculated using equations 3-19 and 3-20 respectively,

$$\delta \dot{Q} = [(I\delta V)^2 + (V\delta I)^2]^{0.5} \quad 3-19$$

$$\delta \dot{q} = \left[ \left( \frac{1}{A} \delta \dot{Q} \right)^2 + \left( -\frac{\dot{Q}}{A^2} \delta A \right)^2 \right]^{0.5} \quad 3-20$$

### 3.9.3.5 Heat transfer coefficient

Using the uncertainties for temperature and heat flux, equation 3-21 can be used to calculate the uncertainty for heat transfer coefficient,

$$\delta h = \left[ \left( \frac{1}{\sqrt{\bar{T}_{inner} - T_b}} \delta \dot{q} \right)^2 + \left( -\frac{\dot{q}}{(\bar{T}_{inner} - T_b)^2} \delta \bar{T}_{inner} \right)^2 + \left( -\frac{\dot{q}}{(\bar{T}_{inner} - T_b)^2} \delta T_b \right)^2 \right]^{0.5} \quad 3-21$$

### 3.9.3.6 Nusselt number and Colburn *j-factor*

Finally the uncertainties for Nusselt number and Colburn *j-factor* are calculated using equations 3-22 and 3-23 respectively,

$$\delta Nu = \left[ \left( \frac{D_i}{k_b} \delta h \right)^2 + \left( \frac{h}{k_b} \delta D_i \right)^2 + \left( -\frac{h D_i}{k_b^2} \delta k_b \right)^2 \right]^{0.5} \quad 3-22$$

$$\delta j = \left[ \left( \frac{1}{Re Pr^{\frac{1}{3}}} \delta Nu \right)^2 + \left( -\frac{Nu}{Re^2 Pr^{\frac{1}{3}}} \delta Re \right)^2 + \left( -\frac{1}{3} \frac{Nu}{Re Pr^{\frac{4}{3}}} \delta Pr \right)^2 \right]^{0.5} \quad 3-23$$

The uncertainty for Nusselt number is summarised graphically over the range of Reynolds numbers in Figure 3.7. The Nusselt number uncertainty remains constant for both pitches and all heat fluxes over the laminar regime at approximately 5%. A sharp increase is seen between 2 000 and 3 000 Reynolds number where the flow enters the transitional regime. The uncertainty then worsens as the flow rate increases as a direct result of a decrease in the temperature rise between the inlet and outlet. For the lowest heat flux, the uncertainty peaks at 31.6% at 7 000 Reynolds but for the highest heat flux the uncertainty peaks much lower at 13.2% at 7 000 Reynolds. The smaller pitch ratio appears to have a worsening effect on uncertainty for the lowest heat flux, which is not evident in the higher heat fluxes.

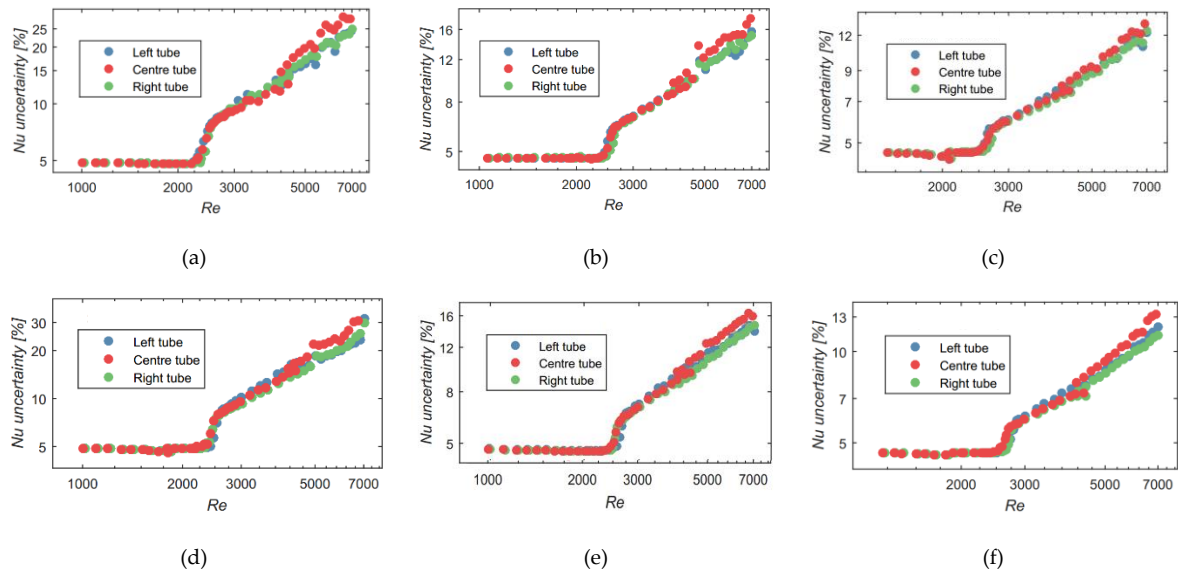


Figure 3.7. The uncertainty for Nusselt number at a pitch of 1.5 for 2, 3 and 4 kW/m<sup>2</sup> is given in (a), (b) and (c) respectively and the uncertainty at a pitch of 1.25 for 2, 3 and 4 kW/m<sup>2</sup> is given in (d), (e) and (f) respectively.

The uncertainty for Colburn  $j$ -factor is summarised graphically in Figure 3.8. The uncertainty for the Colburn  $j$ -factor follows the same trend as the uncertainty for Nusselt number as expected, however it is slightly higher as it considers the uncertainty in both Prandtl number and Reynolds number.

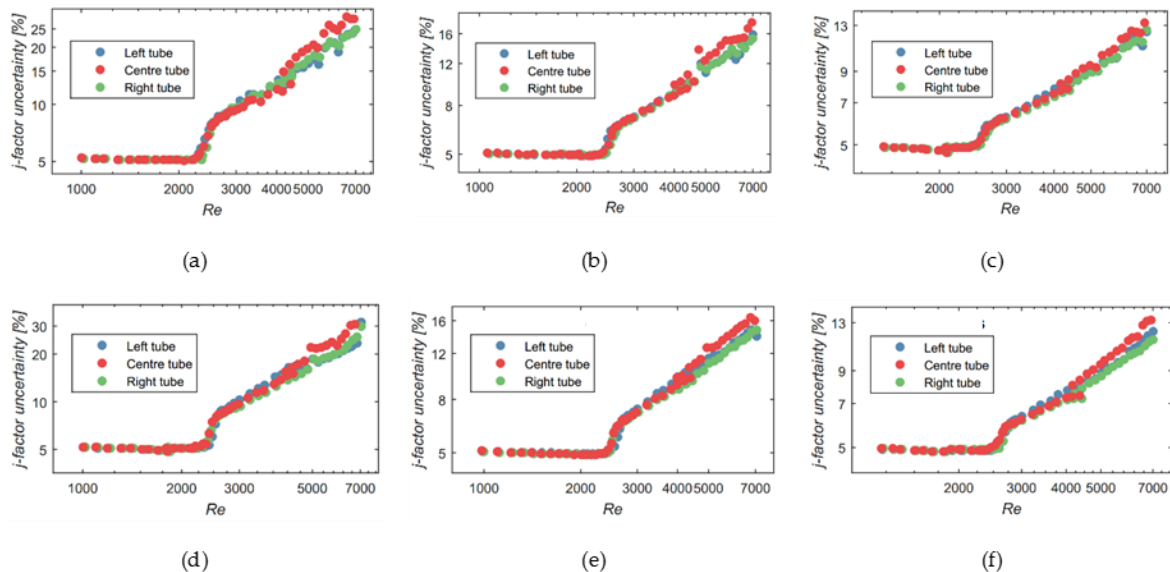


Figure 3.8. The uncertainty for Colburn  $j$ -factor at a pitch of 1.5 for 2, 3 and 4 kW/m<sup>2</sup> is given in (a), (b) and (c) respectively and the uncertainty at a pitch of 1.25 for 2, 3 and 4 kW/m<sup>2</sup> is given in (d), (e) and (f) respectively.

### 3.10 CONCLUSION

The experimental set-up, procedure, data reduction method and uncertainty analysis were discussed in this chapter. The test section was built using three 4 mm inner diameter horizontal smooth tubes each 6 meters in length. A square-edged inlet was achieved by inserting the tubes at pitches of 1.25 and 1.5 times the inner diameter at the outlet of a calming section designed per specification given by Ghajar and Tam (1994). The Reynolds number was varied between 1 000 and 7 000 and water was used as the test fluid. A constant heat flux boundary condition of 2, 3 and 4 kW/m<sup>2</sup> was applied to the tubes using



a direct current power supply that passed current through the stainless-steel tubes. Thirteen thermocouple stations per tube, each consisting of three thermocouples were used to measure the tube wall temperature. PT100 probes at the inlet and outlet were used to measure the bulk fluid temperature. The tubes were adequately insulated to prevent heat loss to the surroundings. A single tube test section was also built and is discussed in Chapter 4. This test section was used for validation of the experimental set up and to compare the effect of the tube pitch ratios.

Methods of data reduction were discussed after which an uncertainty analysis found that the uncertainty for Reynolds number remained below 1.8%. The analysis found that the uncertainty for Nusselt number remained constant at 5% for the laminar regime, and increased as the temperature difference between inlet and outlet decreased. For the lowest heat flux of 2 kW/m<sup>2</sup> and a pitch of 1.25, the Nusselt number uncertainty peaked at 31.6% at 7 000 Reynolds but had a much lower peak of 13.2% for the highest heat flux of 4 kW/m<sup>2</sup>. The uncertainty for Colburn *j-factor* was slightly higher than that of the Nusselt number which is due to the inclusion of Prandtl and Reynolds number uncertainties.

## 4. VALIDATION

### 4.1 INTRODUCTION

To determine whether the experimental set-up can produce accurate and reliable data, a single validation tube was built to compare the results with previous studies. The single tube was built to the same specifications as the three-tube set-up using the same thermocouple locations. The data obtained for the single tube is plotted against both experimental data available in published journals as well as correlations described in section 2.7.

### 4.2 AVERAGE NUSSLETT NUMBER

The result of the uncertainty analysis showed that the experiments at low heat fluxes yielded results where the uncertainty was relatively high – approximately 30%. It is for this reason that a heat flux of 4 kW/m<sup>2</sup> was used for the validation where the maximum uncertainty in Nusselt number over the entire range of Reynolds numbers is a more acceptable 13%. Increasing the heat flux even higher would decrease this uncertainty further, however due to cooling limitations of the experimental set-up for the case of the three-tube set-up, a maximum heat flux of 4 kW/m<sup>2</sup> was used.

The Nusselt number was compared to three correlations – namely the Morcos and Bergles (1975) equation for the laminar regime and the Gnielinski (1976) and Ghajar and Tam (1994) equations for the turbulent regime (see Table 2.1). The results of the experiment are shown graphically in Figure 4.1 showing the laminar, transitional and turbulent regimes.

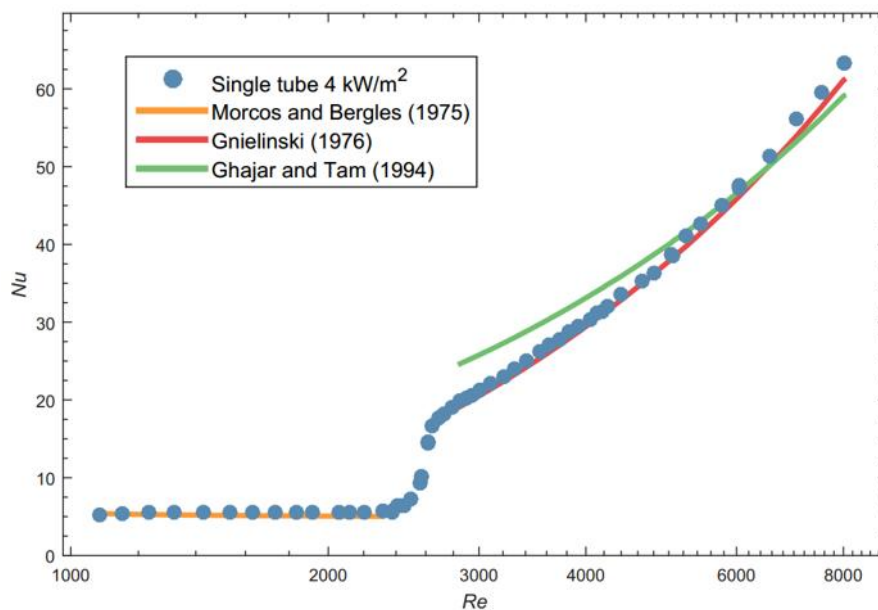


Figure 4.1. Comparison of average Nusselt number for the single tube for fully developed flow at a heat flux of 4 kW/m<sup>2</sup> with correlations available in literature.

The Nusselt number remains constant over the laminar range of Reynolds numbers of 1 100 to 2 200 and deviates from the Morcos and Bergles (1975) equation by an average of 8.1%. At a critical Reynolds number of 2 373, the Nusselt number increases sharply as the flow enters the transitional regime. The flow becomes fully turbulent at a Reynolds number of 2 789 where the Nusselt number deviates from the Gnielinski (1976) equation by an average of 2.7% and deviates from the Ghajar and Tam (1994)

equation by an average of 8.8%. The larger deviation in Nusselt number from the Ghajar and Tam (1994) equation is likely due to the equation only being valid from a Reynolds number of 7 000 upwards.

The average Nusselt number in the laminar regime is 5.54 which is significantly higher than the theoretical value of 4.36. This can be attributed to the effects of secondary flow within the tube. Overall, the experimental results can be said to correlate well with the published equations and confirms the validity of the experimental set-up.

### 4.3 LOCAL NUSSULT NUMBER

For fully developed flow in smooth circular horizontal tubes with a constant heat flux boundary condition, the Nusselt number should remain constant at 4.36 in the laminar regime. Using the flow map provided by Ghajar and Tam (1995), a heat flux of 1 kW/m<sup>2</sup> is used to ensure that the flow is dominated by forced convection and not mixed convection. The critical Reynolds number of 2 109 at this heat flux is shown in Figure 4.2. At this Reynolds number, the theoretical thermal entry length is calculated to be 2.6 meters.

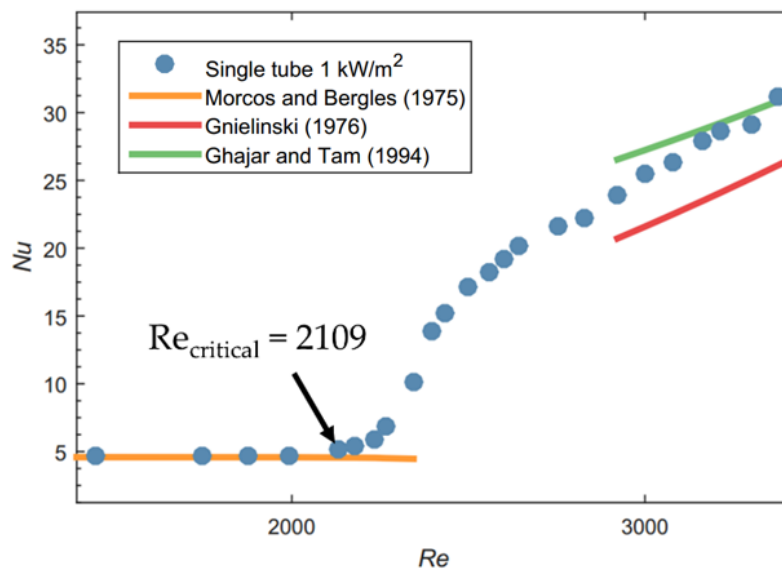


Figure 4.2. Average Nusselt number vs Reynolds number plot for a heat flux of 1 kW/m<sup>2</sup> showing the critical Reynolds number before the flow enters the transitional regime.

The local Nusselt number at a Reynolds number of 2 109 at each thermocouple station is then plotted against  $x/D_i$  as shown in Figure 4.3. Using the theoretical thermal entry length of 2.6 meters, the flow should be fully developed for an  $x/D_i$  of 650 onwards. Figure 4.3 however shows how the flow exhibits the fully developed characteristic much earlier at an  $x/D_i$  of 375.

The local Nusselt correlation of Ghajar and Tam (1994) is also plotted in Figure 4.3 and the average deviation over the range of  $x/D_i$  of 0 to 300 is 7.1% where after the equation is no longer valid. Over the length of the test section which equates to an  $x/D_i$  range of 1 060 to 1 435 the average deviation from the theoretical Nusselt number of 4.36 is 5.4% which shows good correlation and it can be concluded that the forced convection condition is achieved.

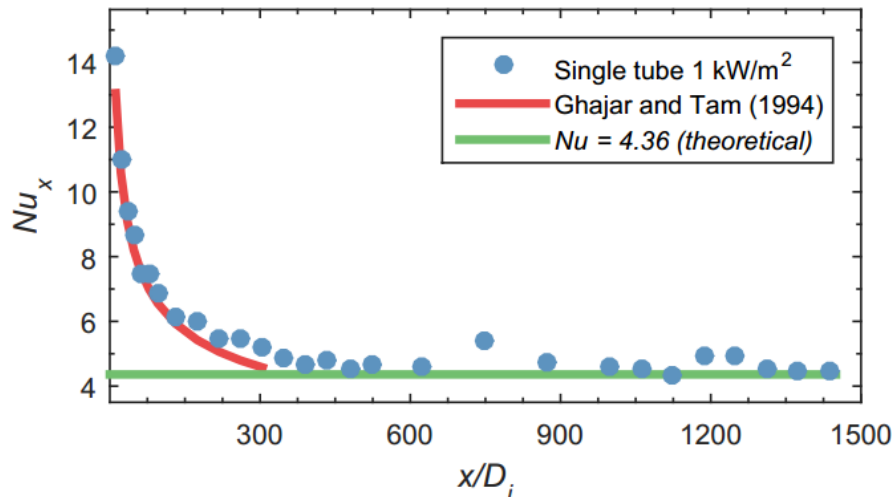


Figure 4.3. Local Nusselt number vs  $x/D_i$  plot for a heat flux of  $1 \text{ kW/m}^2$  at a Reynolds number of 2 109 showing the length of the thermal entry region and the convergence to the theoretical Nusselt number of 4.36.

#### 4.4 CONCLUSION

The experimental set-up and data reduction method for the heat transfer data were validated in this chapter. The average Nusselt numbers were validated against the equation of Morcos and Bergles (1975) in the laminar regime and corresponded well with an average deviation of 8.1%. In the turbulent regime, the average Nusselt numbers deviated from the equation of Gnielinski (1976) by a mere 2.7%.

The local Nusselt numbers at the critical Reynolds number of 2 109 at a heat flux of  $1 \text{ kW/m}^2$  showed good correlation with the equation of Ghajar and Tam (1994) deviating by 7.1% on average in the developing region. For the fully developed region, specifically over the length of the test section the results deviated from the theoretical value of 4.36 by an average 5.4% indicating forced convection conditions were achieved.

The small deviations from theory represent valid data and reliable results can be expected in the experiments for the case of the three-tube set-up.

## 5. RESULTS

### 5.1 INTRODUCTION

Having validated the experimental set-up in the previous chapter, the results for the three-tube set-up are presented. The same manufacturing techniques used in making the single tube were replicated for the case of the three-tube set-up. The tubes were then insulated, and inserted into the calming section attached to the same experimental bench as the single tube. Ensuring a squared-edged inlet condition for the three tubes and a pitch spacing of 1.5 times the outer diameter of 6 mm, the tubes were electrically heated at  $2 \text{ kW/m}^2$  and experiments were conducted for decreasing Reynolds numbers of 7 000 to 1 000. The experiments were repeated for heat fluxes of  $3 \text{ kW/m}^2$  and  $4 \text{ kW/m}^2$  before changing the pitch to 1.25 and repeating all heat fluxes. This chapter contains the average heat transfer results of these experiments, plotted as Nusselt number and Colburn  $j$ -factor against Reynolds number. As a comparison, the data from the single tube is included in the plots.

### 5.2 LAMINAR AND TURBULENT HEAT TRANSFER RESULTS FOR A PITCH OF 1.5

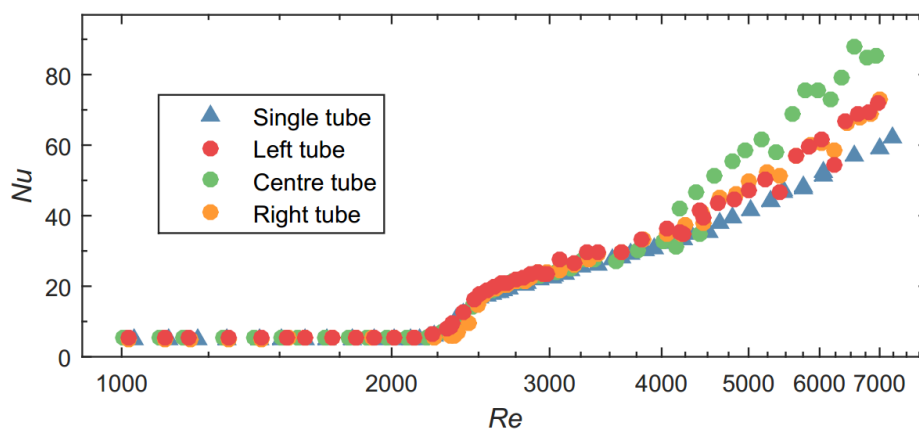
The Nusselt number and Colburn  $j$ -factor are calculated for each heat flux at a pitch of 1.5 and plotted against Reynolds number. This section is split into subsections to discuss the influence of each heat flux.

#### 5.2.1 $2 \text{ kW/m}^2$ heat flux

Figure 5.1 shows the average Nusselt number and Colburn  $j$ -factor plotted against Reynolds number for the single and three-tube set-up for a heat flux of  $2 \text{ kW/m}^2$ . The plots to show flow transition from laminar at a Reynolds number of approximately 2 200.

The average Nusselt number for the three-tube set-up shows good correlation to that of the single tube set-up particularly in the laminar regime. The left, centre and right tubes deviate from the single tube by an average of 7.9%, 9.4% and 6.1% respectively. The Nusselt number deviation from the single tube worsens in the turbulent regime as a result of the uncertainty increasing and was found to deviate by 13.1%, 23.9% and 12.9% respectively.

The average Colburn  $j$ -factor for the three tubes also shows good correlation and was found to deviate by 6.7%, 7.4% and 4.9% in the laminar regime and by 12.3%, 23.1% and 12.1% in the turbulent regime for the left, centre and right tubes respectively.



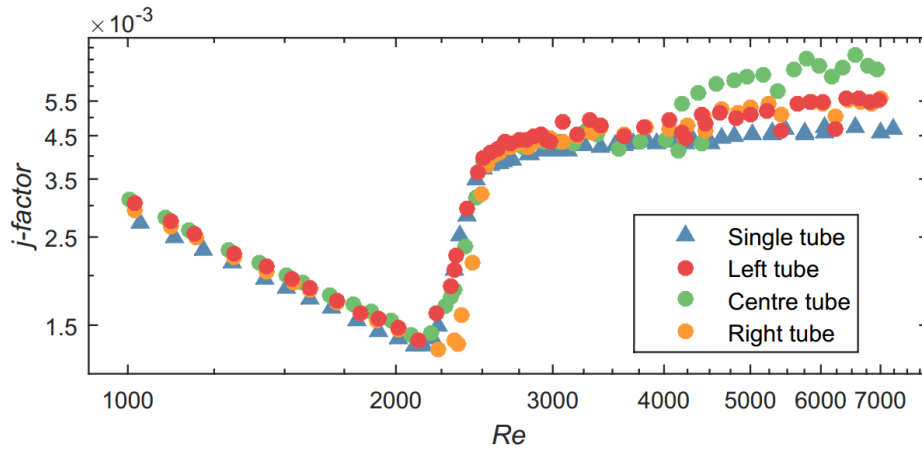


Figure 5.1. Average Nusselt number (top) and Colburn  $j$ -factor (bottom) plotted against Reynolds number for the single and three-tube set-up for a heat flux of  $2 \text{ kW/m}^2$  and a pitch of 1.5.

### 5.2.2 $3 \text{ kW/m}^2$ heat flux

Figure 5.2 shows the average Nusselt number and Colburn  $j$ -factor plotted against Reynolds number for the single and three-tube set-up for a heat flux of  $3 \text{ kW/m}^2$ . The onset of transition is seen to be delayed when compared to the heat flux of  $2 \text{ kW/m}^2$  and occurs at a Reynolds number of approximately 2 300.

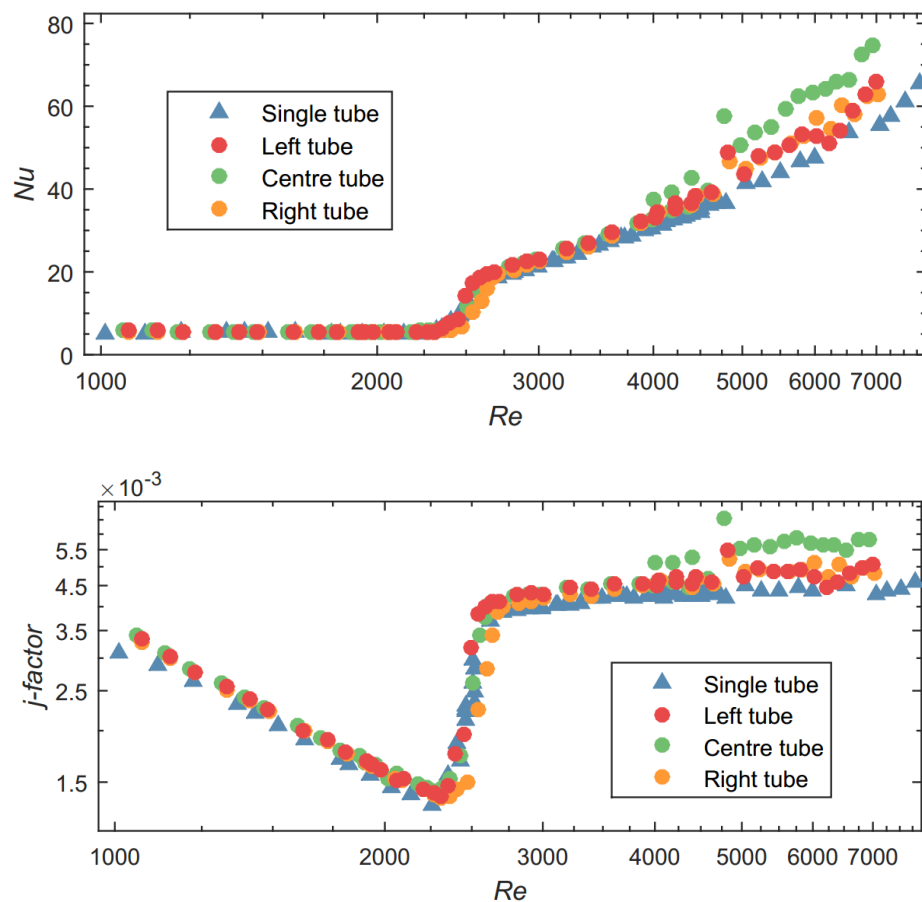


Figure 5.2. Average Nusselt number (top) and Colburn  $j$ -factor (bottom) plotted against Reynolds number for the single and three-tube set-up for a heat flux of  $3 \text{ kW/m}^2$  and a pitch of 1.5.

The average Nusselt number for the left, centre and right tubes again shows good correlation with the single tube data and deviates by 7.6%, 8.1% and 7.0% respectively in the laminar regime, which is similar compared to the deviation in this regime for the 2 kW/m<sup>2</sup> heat flux case. The deviation in the turbulent regime was however better at 10.4%, 21.3% and 10.0% for the left, centre and right tubes respectively and can be attributed to the lower uncertainties at this heat flux.

The average Colburn  $j$ -factor for the three tubes exhibit the same trend in deviation from the single tube, and was found to be 7.2%, 7.1% and 6.5% in the laminar regime and 9.4%, 20.1% and 9.0% in the turbulent regime for the left, centre and right tubes respectively.

### 5.2.3 4 kW/m<sup>2</sup> heat flux

Figure 5.3 shows the average Nusselt number and Colburn  $j$ -factor plotted against Reynolds number for the single and three-tube set-up for a heat flux of 4 kW/m<sup>2</sup>. Transition can be seen to have started at a Reynolds number of approximately 2 400.

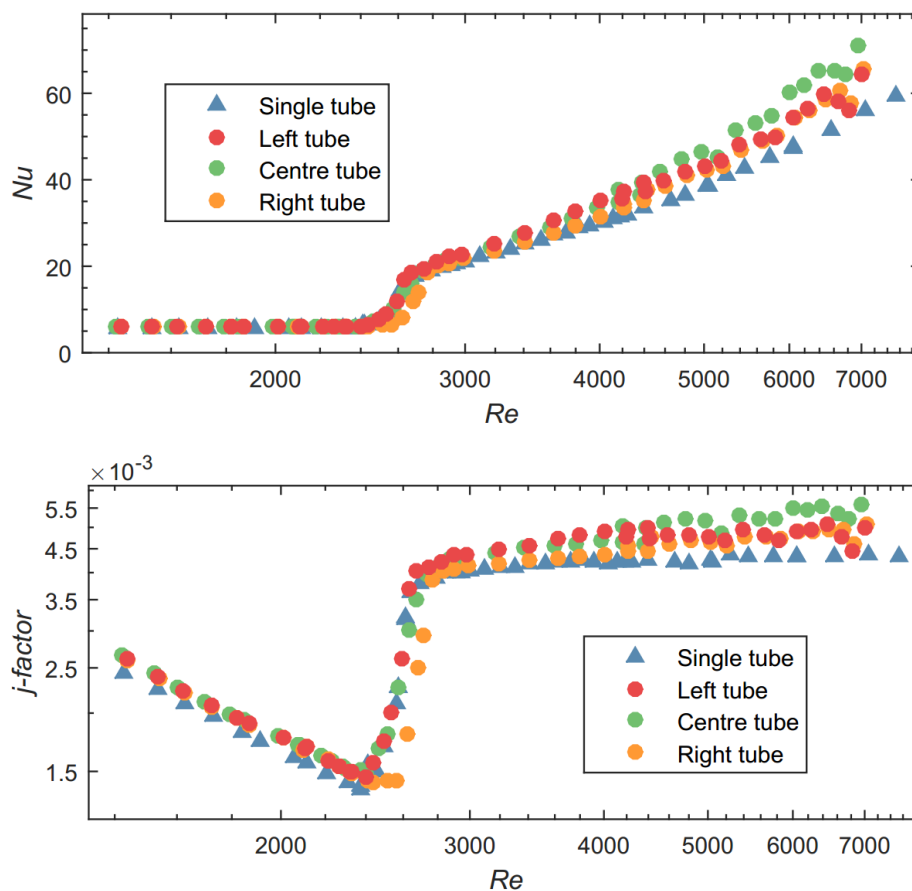


Figure 5.3. Average Nusselt number (top) and Colburn  $j$ -factor (bottom) plotted against Reynolds number for the single and three-tube set-up for a heat flux of 4 kW/m<sup>2</sup> and a pitch of 1.5.

The Nusselt number deviations for the left, centre and right tubes from the single tube were found to be 7.8%, 8.4% and 7.5% respectively in the laminar regime and due to the lower uncertainties at this heat flux, deviations are 13.0%, 17.8% and 8.7% respectively in the turbulent regime.

The same trend was found for the  $j$ -factor. The left, centre and right tube  $j$ -factor deviated from the single tube by 8.0%, 7.8% and 7.6% in the laminar regime and 12.5%, 17.4% and 8.1% in the turbulent regime which is lower than the previous two heat fluxes.

### 5.3 TRANSITIONAL HEAT TRANSFER RESULTS FOR A PITCH OF 1.5

The Nusselt number and Colburn  $j$ -factor are calculated for each heat flux at a pitch of 1.5 and again plotted against Reynolds number. A zoomed view of the transitional regime is provided for each heat flux.

#### 5.3.1 2 kW/m<sup>2</sup> heat flux

Figure 5.4 shows a zoomed view of the transitional region for a heat flux of 2 kW/m<sup>2</sup> and a pitch of 1.5. The critical Reynolds number for each tube is indicated in the plot, and it was found that the flow entered the transitional regime at a Reynolds number of approximately 2 200.

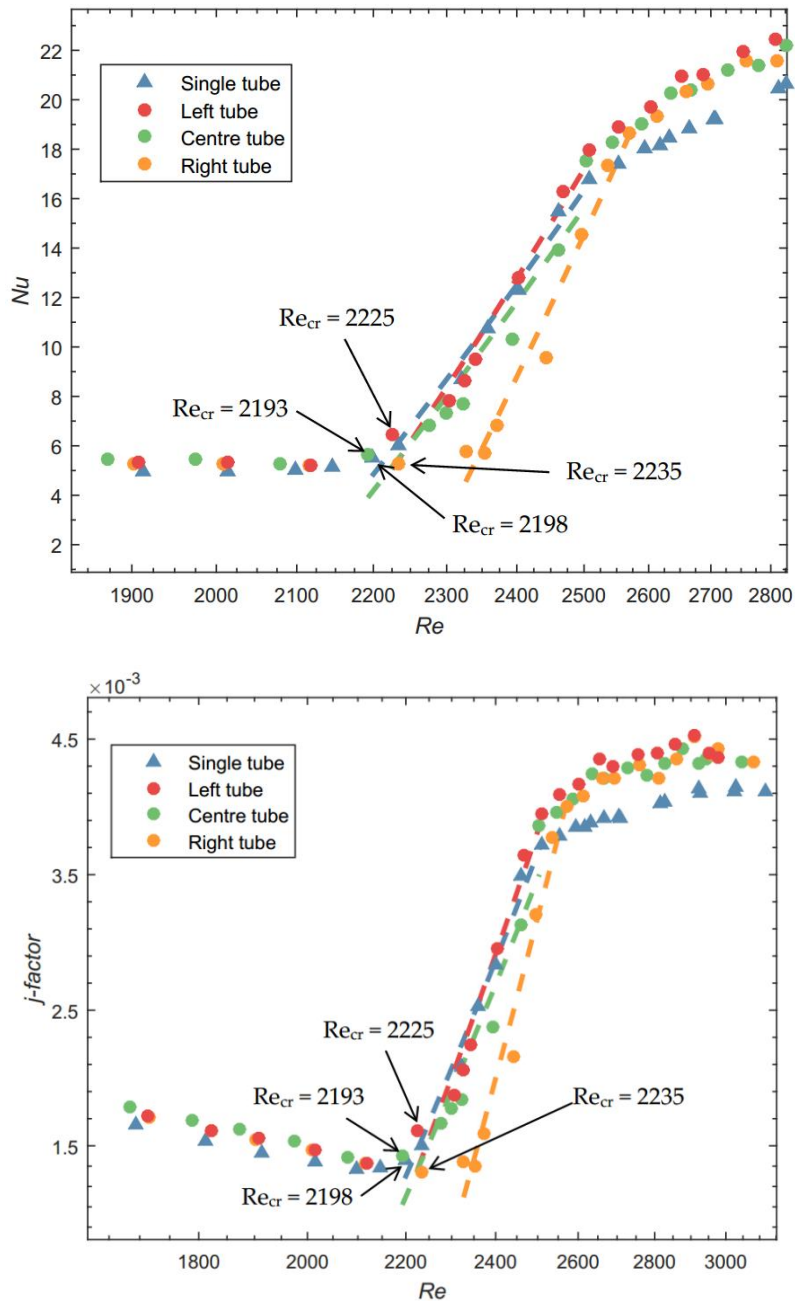


Figure 5.4. Transitional average Nusselt number (top) and Colburn  $j$ -factor (bottom) plotted against Reynolds number for the single and three-tube set-up for a heat flux of 2 kW/m<sup>2</sup> and a pitch of 1.5.

The gradient of the transitional region was identical for the single tube and the left and centre tubes, with the right tube having a slightly sharper gradient. Although the flow in the right tube enters the transitional regime at a similar Reynolds number to the other tubes, it appears to stay in the lower end of transition for a longer range of Reynolds numbers. All tubes appear to be in the turbulent regime from a Reynolds number of 2 600 onwards and it appears that the presence of the three tubes at the inlet did not have a significant effect on either the Nusselt number or Colburn  $j$ -factor at a heat flux of 2 kW/m<sup>2</sup>.

### 5.3.2 3 kW/m<sup>2</sup> heat flux

Figure 5.5 shows a zoomed view of the Nusselt number and Colburn  $j$ -factor in the transitional regime for a heat flux of 3 kW/m<sup>2</sup> and a pitch of 1.5.

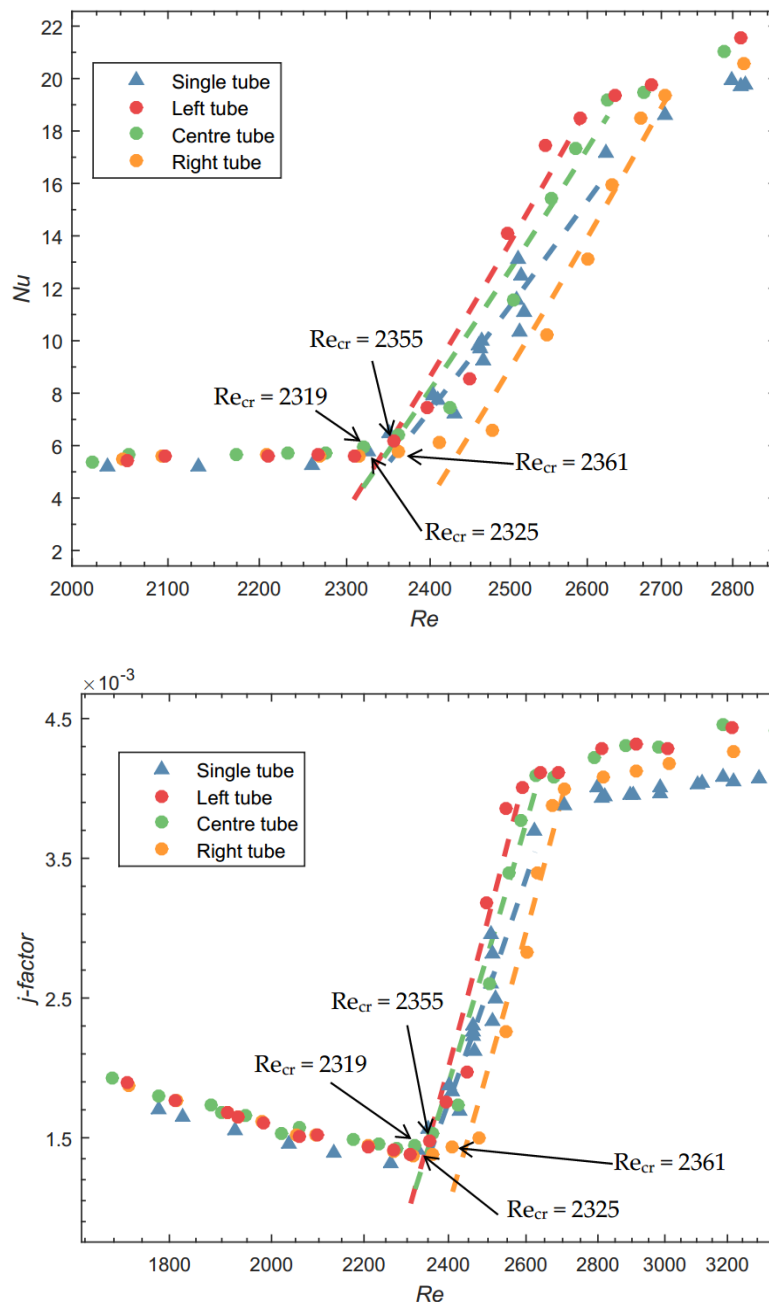


Figure 5.5. Transitional average Nusselt number (top) and Colburn  $j$ -factor (bottom) plotted against Reynolds number for the single and three-tube set-up for a heat flux of 3 kW/m<sup>2</sup> and a pitch of 1.5.

A similar trend to the previous heat flux is noticed. The presence of multiple tubes appears to have no significant effect on either Nusselt number or  $j$ -factor in the transitional region. The flow for all three tubes was said to be in the transitional regime for a Reynolds number of approximately 2 300 with the right tube exhibiting a similar behaviour as for the heat flux of 2 kW/m<sup>2</sup> and remaining in the lower transitional regime for a broader range of Reynolds numbers. The gradient of the line for the Nusselt number and  $j$ -factor is again less steep for the right tube.

### 5.3.3 4 kW/m<sup>2</sup> heat flux

Figure 5.6 shows a zoomed view of the Nusselt number and Colburn  $j$ -factor in the transitional regime for a heat flux of 4 kW/m<sup>2</sup> and a pitch of 1.5.

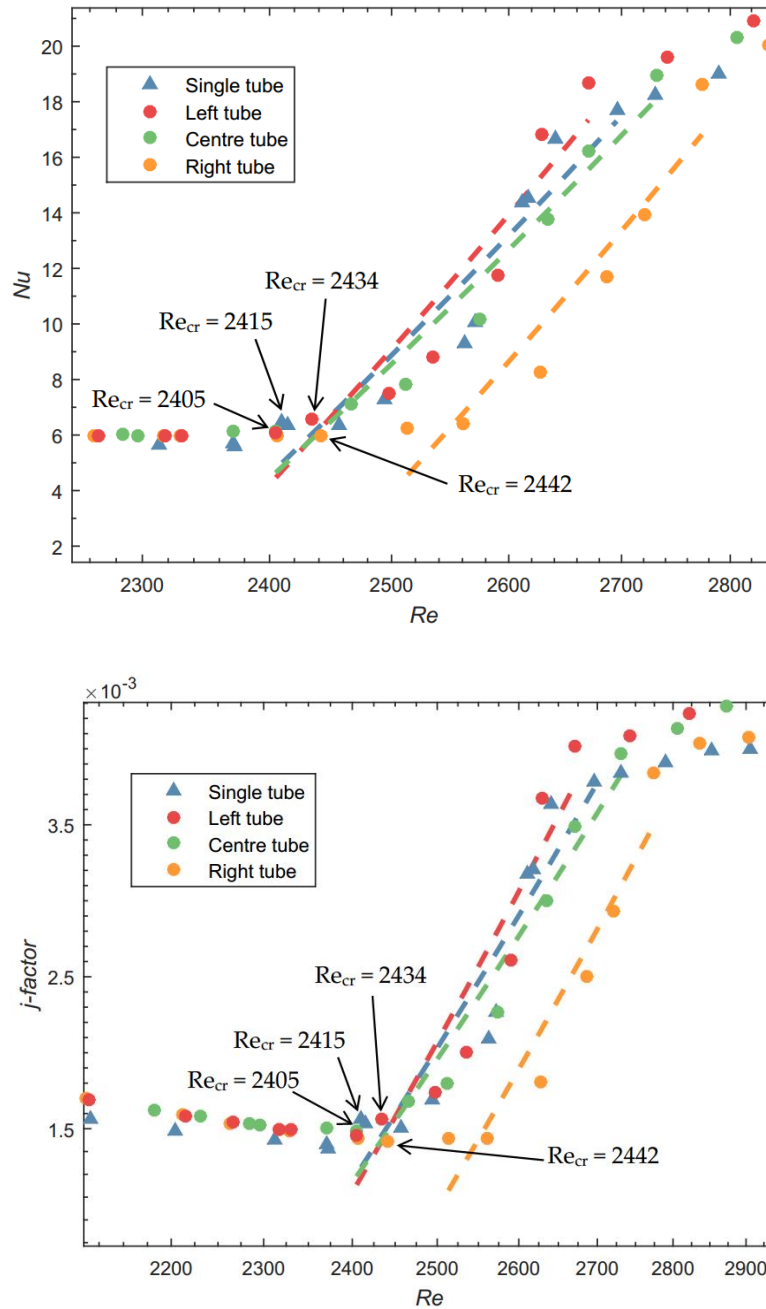


Figure 5.6. Transitional average Nusselt number (top) and Colburn  $j$ -factor (bottom) plotted against Reynolds number for the single and three-tube set-up for a heat flux of 4 kW/m<sup>2</sup> and a pitch of 1.5.

The increase in heat flux increases the critical Reynolds number to approximately 2 400 for all tubes. The critical Reynolds number and gradient of the transitional regime for the left, centre and single tubes were similar and again the right tube appears to exhibit a delayed response. The right tube had a slightly higher critical Reynolds number of 2 442 and remained in the lower transitional regime for a longer range of Reynolds numbers. This caused the gradient of the transitional regime to be steeper.

## 5.4 LAMINAR AND TURBULENT HEAT TRANSFER RESULTS FOR A PITCH OF 1.25

The Nusselt number and Colburn  $j$ -factor are calculated for each heat flux at a pitch of 1.25 and plotted against Reynolds number. The section is again split to discuss the influence of each heat flux.

### 5.4.1 2 kW/m<sup>2</sup> heat flux

Figure 5.7 shows the average Nusselt number and Colburn  $j$ -factor plotted against Reynolds number for the single and three-tube set-up for a heat flux of 2 kW/m<sup>2</sup>. The change in pitch ratio did not seem to influence the onset of transition for the centre tube, and the flow appeared to be in the transitional regime from a Reynolds number of 2 200.

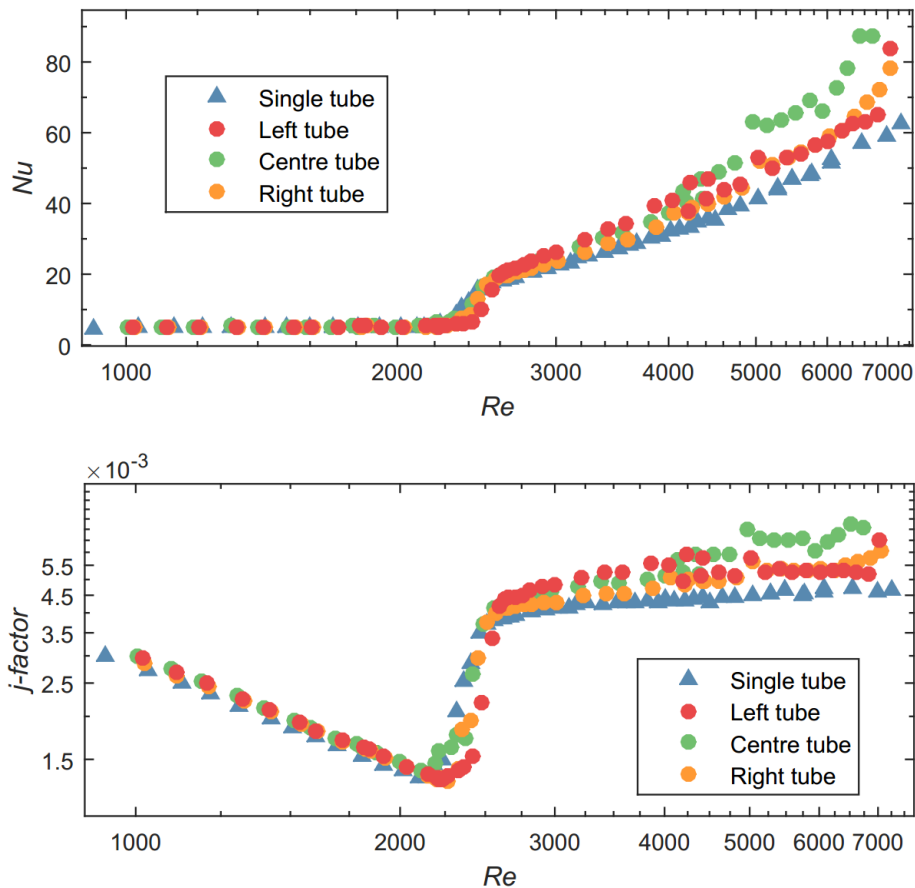


Figure 5.7. Average Nusselt number (top) and Colburn  $j$ -factor (bottom) plotted against Reynolds number for the single and three-tube set-up for a heat flux of 2 kW/m<sup>2</sup> and a pitch of 1.25.

The average Nusselt number in the laminar regime for the left, centre and right tubes deviates from the single tube data by 7.2%, 7.5% and 6.0% respectively which is comparable to the previous pitch ratio of 1.5. The deviation worsens again in the turbulent regime where the uncertainty is high and was found to be 20.1%, 32.9% and 14.1% for the left, centre and right tubes respectively.

The deviation for the  $j$ -factor however improved and was found to be 3.6%, 3.2% and 2.5% for the left, centre and right tubes in the laminar regime which shows good correlation with the single tube data.

However, in the turbulent regime the deviation from the single tube data was 20.7%, 34.1% and 14.6% for the left, centre and right tubes. This large deviation is attributed to the high uncertainty associated with this heat flux.

#### 5.4.2 3 kW/m<sup>2</sup> heat flux

Figure 5.8 shows the average Nusselt number and Colburn  $j$ -factor plotted against Reynolds number for the single and three-tube set-up for a heat flux of 3 kW/m<sup>2</sup>. The flow appeared to be in the transitional regime from a Reynolds number of 2 300.

Figure 5.8 shows good correlation again for the Nusselt number of the left, centre and right tubes in the laminar regime and deviates from the single tube data by 7.4%, 8.0% and 6.75% respectively. With the decrease in uncertainty at this heat flux, a decrease in deviation in the turbulent regime was noticed – 12.6%, 19.0% and 6.3% for the left, centre and right tubes respectively.

The  $j$ -factor for the left, centre and right tubes deviated from the single tube data by 5.54%, 5.89% and 5.0% respectively in the laminar regime and worsened to 12.52%, 19.3% and 6.3% respectively in the turbulent regime.

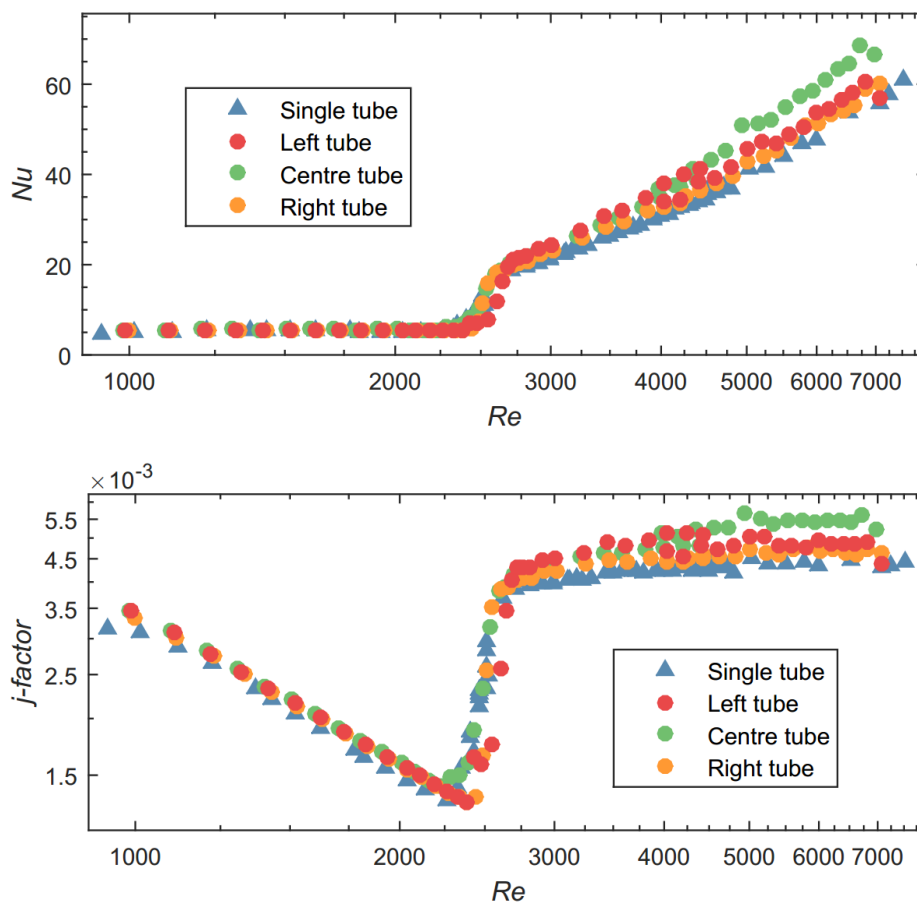


Figure 5.8. Average Nusselt number (top) and Colburn  $j$ -factor (bottom) plotted against Reynolds number for the single and three-tube set-up for a heat flux of 3 kW/m<sup>2</sup> and a pitch of 1.25.

#### 5.4.3 4 kW/m<sup>2</sup> heat flux

Figure 5.9 shows the average Nusselt number and Colburn  $j$ -factor plotted against Reynolds number for the single and three-tube set-up for a heat flux of 4 kW/m<sup>2</sup>. Transition is again delayed due to the increased heat flux and is said to be in the transitional regime from a Reynolds number of

approximately 2 400. The higher heat flux at this pitch ratio appears to influence the critical Reynolds number of the left and right tubes.

The deviation of the left, centre and right tubes from the single tube was found to be 8.1%, 9.8% and 8.2% respectively in the laminar regime and 12.2%, 18% and 5.5% respectively in the turbulent regime. Whilst the deviation in the laminar regime was higher than that of the previous two heat fluxes at this pitch, the deviation in the turbulent regime was comparable to the previous heat flux.

The  $j$ -factor for the left, centre and right tubes was found to deviate from the single tube data by 5.8%, 7.0% and 5.81% respectively in the laminar regime and 11.4%, 17.5% and 4.7% respectively in the turbulent regime.

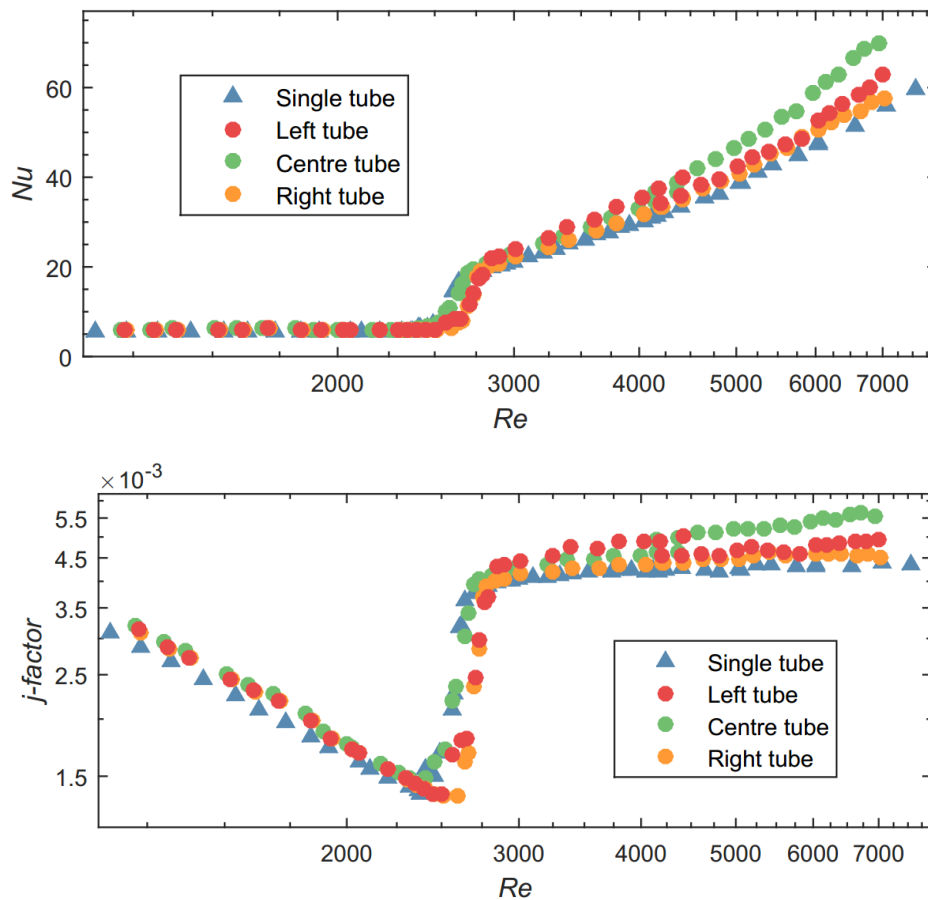


Figure 5.9. Average Nusselt number (top) and Colburn  $j$ -factor (bottom) plotted against Reynolds number for the single and three-tube set-up for a heat flux of  $4 \text{ kW/m}^2$  and a pitch of 1.25.

## 5.5 TRANSITIONAL HEAT TRANSFER RESULTS FOR A PITCH OF 1.25

The Nusselt number and Colburn  $j$ -factor are calculated for each heat flux at a pitch of 1.25 and again plotted against Reynolds number. A zoomed view of the transitional regime is provided for each heat flux.

### 5.5.1 $2 \text{ kW/m}^2$ heat flux

Figure 5.10 shows a zoomed view of the Nusselt number and Colburn  $j$ -factor in the transitional regime for a pitch of 1.25 and a heat flux of  $2 \text{ kW/m}^2$ . Again, the flow in the single and centre tubes entered the transitional regime at a Reynolds number of approximately 2 150. However, the left and right tubes

exhibited a delayed response and entered the transitional regime at a higher Reynolds number of approximately 2 260.

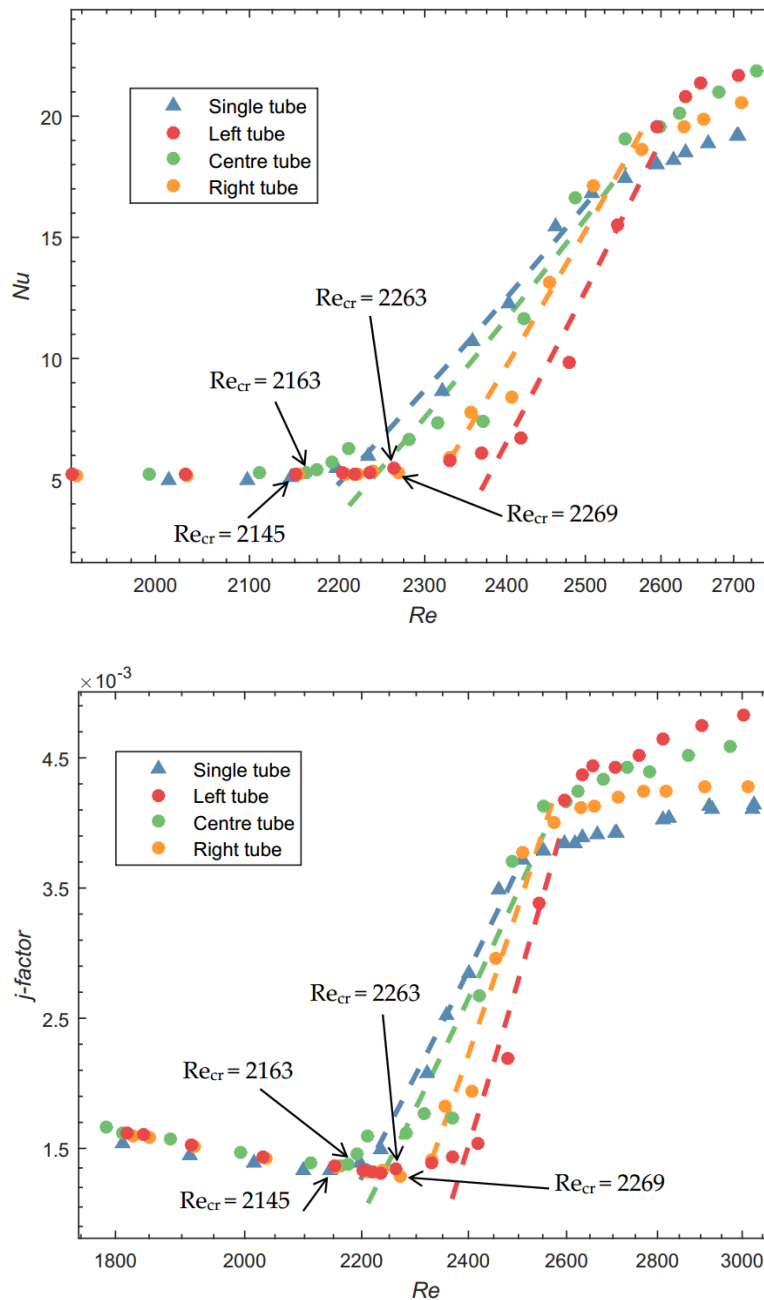


Figure 5.10. Transitional average Nusselt number (top) and Colburn  $j$ -factor (bottom) plotted against Reynolds number for the single and three-tube set-up for a heat flux of 2 kW/m<sup>2</sup> and a pitch of 1.25.

The gradient of the transitional regime for both  $j$ -factor and Nusselt number was similar for the left and right tubes and appeared steeper than that of the centre and single tubes. All tubes appear to be turbulent from a Reynolds number of approximately 2 600 onwards and the presence of multiple tubes appears to delay the onset of transition for the outermost tubes without affecting the centre tube.

### 5.5.2 3 kW/m<sup>2</sup> heat flux

Figure 5.11 shows the Nusselt number and  $j$ -factor for the single, left, centre and right tubes over the transitional regime at a heat flux of 3 kW/m<sup>2</sup> and at a pitch of 1.25.

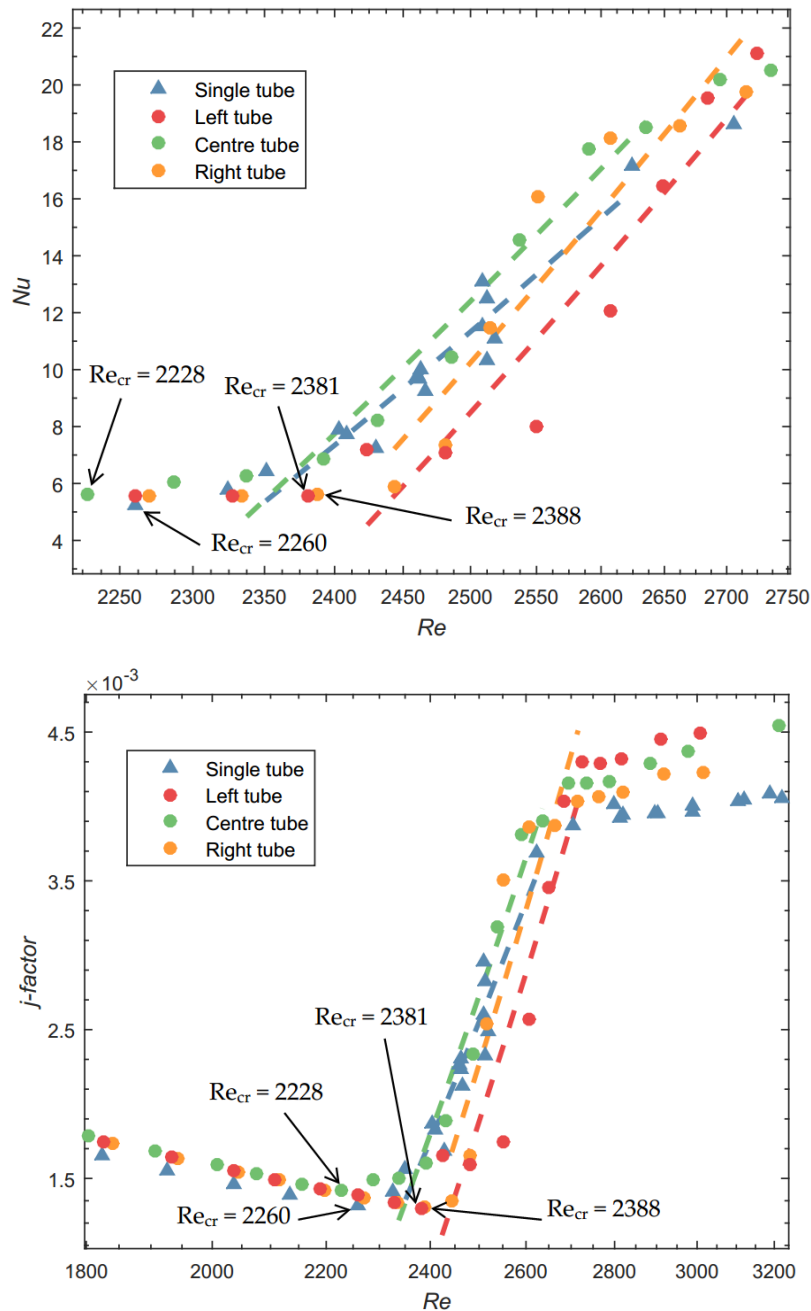


Figure 5.11. Transitional average Nusselt number (top) and Colburn  $j$ -factor (bottom) plotted against Reynolds number for the single and three-tube set-up for a heat flux of  $3 \text{ kW/m}^2$  and a pitch of 1.25.

It was again noticed that the centre tube showed good correlation with the trend of the single tube, and entered the transitional regime at a Reynolds number of approximately 2 250. The left and right tubes exhibited the same behaviour as with the previous heat flux, and the transitional regime was delayed as the tubes entered the transitional regime at a significantly higher Reynolds number of approximately 2 380. The flow for all tubes appeared to be turbulent from a Reynolds number of 2 700, which again made the gradient of the transitional regime for the left and right tubes steeper.

### 5.5.3 $4 \text{ kW/m}^2$ heat flux

Figure 5.12 shows the Nusselt number and  $j$ -factor for the single, left, centre and right tubes over the transitional regime at a heat flux of  $4 \text{ kW/m}^2$  and at a pitch of 1.25.

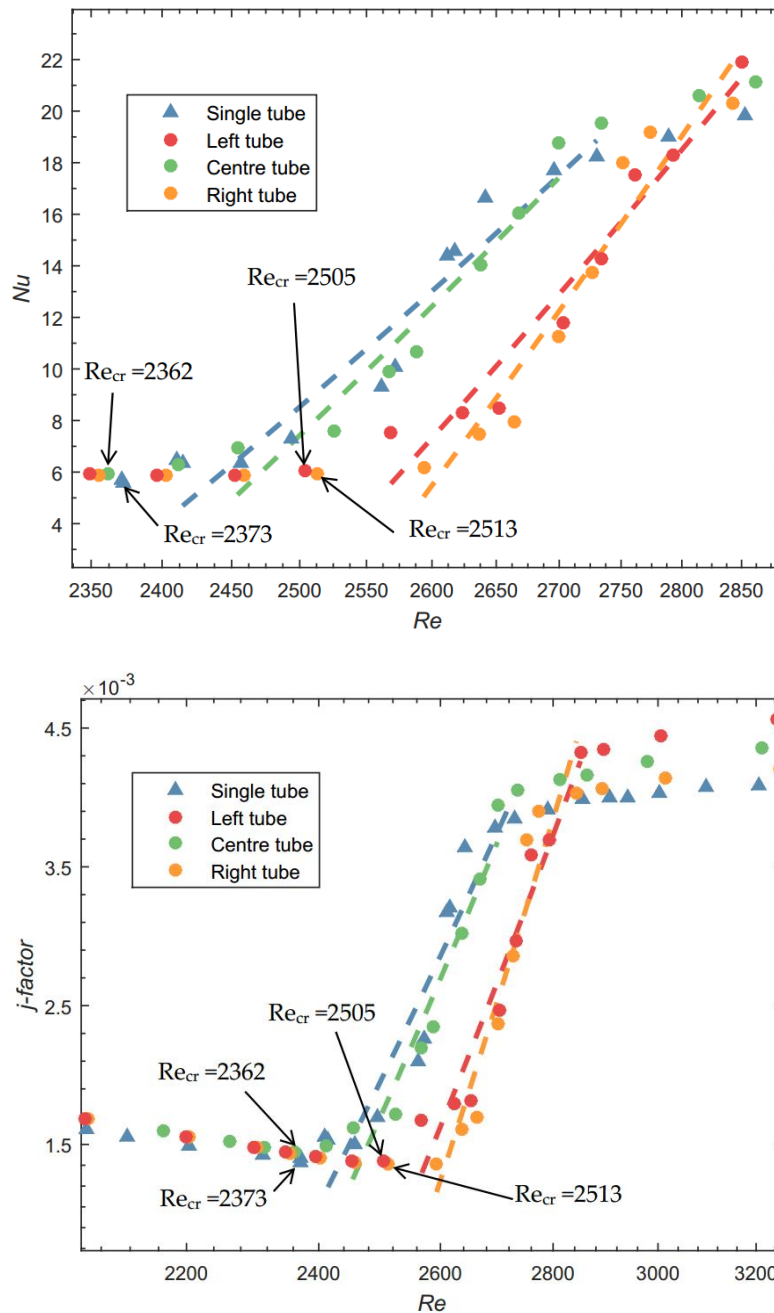


Figure 5.12. Transitional average Nusselt number (top) and Colburn  $j$ -factor (bottom) plotted against Reynolds number for the single and three-tube set-up for a heat flux of  $4\text{ kW/m}^2$  and a pitch of 1.25.

The same trend was noticed as with the previous two heat fluxes. The presence of multiple tubes delays the onset of transition for the left and right tubes as they enter the transitional regime at a Reynolds number of approximately 2 500 whereas the centre tube follows the profile of the single tube and enters the transitional regime at a Reynolds number of approximately 2 360. A notable difference at this heat flux was the delay in onset of the turbulent regime. The centre tube followed the trend of the single tube and was turbulent from a Reynolds number of 2 700 onwards whereas the left and right tube appeared to be turbulent from a Reynolds number of 2 800.



## 5.6 COMPARISON OF RESULTS

Table 5.1 shows the critical Reynolds numbers for the left, centre and right tubes at tube pitch ratios of 1.5 and 1.25 for heat fluxes of 2 kW/m<sup>2</sup>, 3 kW/m<sup>2</sup> and 4 kW/m<sup>2</sup>.

Table 5.1. Critical Reynolds numbers (start of the transitional regime) for the left, centre and right tubes at varying pitches and heat fluxes.

	2 kW/m <sup>2</sup>		3 kW/m <sup>2</sup>		4 kW/m <sup>2</sup>	
	Pitch 1.5	Pitch 1.25	Pitch 1.5	Pitch 1.25	Pitch 1.5	Pitch 1.25
Left tube	2 225	2 263	2 355	2 381	2 434	2 505
Centre tube	2 193	2 163	2 319	2 228	2 405	2 362
Right tube	2 235	2 269	2 361	2 388	2 442	2 513

This table shows that multiple tubes at the inlet for a tube pitch ratio of 1.5 had no significant effect on the onset of transition. However, at a pitch of 1.25 the left and right tubes experienced a delay in the onset of transition, which increased with increasing heat flux.

Table 5.2 compares the slope of the transitional regime for the left, centre and right tubes for both pitches and all heat fluxes. As previously noted, the smaller pitch ratio of 1.25 appeared to increase the gradient of the transitional regime when compared to the larger pitch ratio of 1.5. This effect is amplified with increasing heat flux.

Table 5.2. Transitional regime gradient for the left, centre and right tubes at varying pitches and heat fluxes.

	2 kW/m <sup>2</sup>		3 kW/m <sup>2</sup>		4 kW/m <sup>2</sup>	
	Pitch 1.5	Pitch 1.25	Pitch 1.5	Pitch 1.25	Pitch 1.5	Pitch 1.25
Left tube	0.0403	0.0583	0.0515	0.0510	0.0485	0.0553
Centre tube	0.0384	0.0411	0.0461	0.0463	0.0410	0.0491
Right tube	0.0591	0.0534	0.0494	0.0531	0.0473	0.0674

The left, centre and right tubes however appeared to end transition at similar Reynolds numbers at both the pitch of 1.5 and 1.25 concluding that the delayed effect is limited to the start of transition at a pitch of 1.25.

## 5.7 CONCLUSION

The chapter discussed the results of the experiment into determining the effect of a multiple tube inlet condition on heat transfer characteristics in the transitional flow regime. The experiments were conducted for pitch ratios of 1.5 and 1.25 and at three heat fluxes – 2 kW/m<sup>2</sup>, 3 kW/m<sup>2</sup> and 4 kW/m<sup>2</sup> and included data capture in the laminar, transitional and turbulent regimes. The results were presented in terms of the average Nusselt number and Colburn *j-factor* plotted against a range of Reynolds number from 1 000 to 7 000.

The laminar results for both pitch ratios and at all heat fluxes showed that the left, centre and right tubes correlated well with the data obtained from the single tube set up. Both the Nusselt number and Colburn *j-factor* were found to deviate by less than 10% on average from the single tube data in the laminar regime. The presence of multiple tubes at the inlet appeared to have little to no effect on the heat transfer characteristics in the laminar regime – irrespective of heat flux or tube pitch ratio. It was however noticed that the heat transfer increased for increasing heat flux in the laminar regime, which can be attributed to mixed convection due to secondary flow.



The turbulent results showed on average a much higher deviation in results between the left, centre and right tubes and the single tube which can be attributed to the higher uncertainties associated with this regime. For the lower turbulent regime where the uncertainty was acceptably low, the effect of multiple tubes on the heat transfer characteristics was negligible – irrespective of heat flux or tube pitch ratio. The flow became fully turbulent at higher Reynolds numbers for increasing heat flux.

The transitional regime results for a pitch of 1.5 showed little to no effect caused by the presence of multiple tubes at the inlet. The right tube appeared to exhibit a prolonged period in the lower transitional region however the critical Reynolds number did not significantly differ from the single, left or centre tubes. This phenomenon can possibly be attributed to tube geometry. The result of this behaviour caused the right tube to experience a much sharper transition gradient for all heat fluxes at the pitch of 1.5.

The transitional regime results for a pitch of 1.25 showed a significant effect on the onset of transition for the left and right tubes, which was amplified with increasing heat flux.

## 6. SUMMARY, CONCLUSIONS AND RECOMMENDATIONS

### 6.1 SUMMARY

The ever-increasing need for the supply of energy for a population that is projected to reach 9 billion within the next 25 years is a major concern for modern engineers. This has led to new and more sustainable alternatives to the conventional and out-dated use of fossil fuels for electricity generation. The South African climate lends itself favourably in the argument towards the use of solar systems, such as concentrated solar power (CSP). A key design concern for the majority of renewable energy systems is efficiency - where the renewable alternative needs to be at least as economically viable as the fossil fuel systems in initial capital cost, cost of operation and potential energy yield.

In any energy generation facility, heat exchangers as a heat transfer mechanism between fluids are used extensively. Research into heat transfer characteristics of flow within horizontal circular tubes has been conducted since the 19<sup>th</sup> century. In an effort to increase the overall efficiency of these heat exchangers, extensive research has recently been conducted into flow in the transitional regime. The transitional regime represents a favourable trade-off between the laminar and turbulent regimes – offering a higher heat transfer coefficient than in the laminar regime and a lower pressure drop than in the turbulent regime.

Correlations for flow in the transitional regime for horizontal circular tubes with varying inlet geometries were developed and have presented experimental results for enhanced tubes, nanofluids and micro-channels. Recent research has also been published into characterising the flow in the developing region. However, these studies have focused on single tubes and have not investigated the effect of multiple tubes at the inlet as found in the case of shell-and-tube heat exchangers. A gap in literature was thus identified and laid the foundation for the experimental work in this dissertation.

An experimental set-up was designed and built to investigate the effect of multiple tubes at the inlet on heat transfer characteristics, with specific focus on the transitional regime. A calming section based on the work of Ghajar and Tam (1994) was built using PVC and cast epoxy. A single tube set-up was built for validation purposes and compared to available literature. The stainless-steel tube had an inner diameter of 4 mm, wall thickness of 1 mm and measured 6 meters in length. A three-tube set-up was then built to the same specification as the single tube set-up, and inserted into the test section at pitch ratios of 1.25 and 1.5 times the outer diameter of the tube. Using PT100 probes and thermocouples at the inlet, outlet and outer surface of the heat exchanger the heat transfer characteristics were experimentally investigated for the fully developed region of the tube. Three DC power supplies were used to heat the tubes at a constant heat flux of 2 kW/m<sup>2</sup>, 3 kW/m<sup>2</sup> and 4 kW/m<sup>2</sup>.

An uncertainty analysis for the heat transfer characteristics concluded that the average Nusselt number uncertainty over the laminar region remained below 5%, but increased to over 30% in the upper turbulent regime as a result of the lower temperature increase over the length of the heat exchanger at increased mass flow rates. In the transitional regime, which was the region of interest in this dissertation, the maximum average Nusselt number uncertainty did not exceed 8%.

### 6.2 CONCLUSIONS

The results over the range of Reynolds numbers of 1 000 to 7 000 show that the laminar and turbulent heat transfer characteristics were negligibly influenced by the presence of multiple tubes at the inlet at either pitch ratio.



In the laminar regime, the Nusselt number and Colburn  $j$ -factor follow the same trend as the data obtained for the single validation tube which was shown to correlate well with available literature. In the turbulent regime, the uncertainties become high and result in a more significant deviation in results when compared to the single tube data.

In the transitional regime at a pitch of 1.5, the left, centre and right tubes underwent transition at a similar critical Reynolds number, however the right tube exhibited a behaviour that saw the flow remain in the lower end of the transitional regime for a prolonged period. This phenomenon increased the transition gradient for this tube. The end of the transitional regime appeared to be unaffected for all three tubes at this pitch, irrespective of heat flux which leads to the conclusion that the heat transfer characteristics in the transitional regime were negligibly affected by the presence of adjacent tubes at a pitch of 1.5 at the inlet.

The heat transfer characteristics at a pitch of 1.25 showed a delay in onset of the transitional regime for the outermost tubes – namely the left and right tubes at all three heat fluxes. The transitional regime was shown to be delayed by a Reynolds number of up to 71 when compared with the pitch ratio of 1.5 which translates to a 3% delay. This delay in the onset of transition appeared to increase with increasing heat flux. The centre tube appeared to follow the trend of the single tube data and the onset of transition appears to be promoted. The end of transition appeared to only be affected at a heat flux of 4 kW/m<sup>2</sup>, which increased the transition gradient for the left and right tubes at heat fluxes of 2 kW/m<sup>2</sup> and 3 kW/m<sup>2</sup>.

The results presented in this dissertation could aid shell-and-tube heat exchanger designers in their design of a heat exchanger with a similar configuration. With further investigation into this type of inlet condition, it is possible that heat exchangers may operate with higher overall efficiencies and help promote the use of renewable energy systems such as concentrated solar power for electricity generation for future generations.

### 6.3 RECOMMENDATIONS

- Larger diameter tubes which would more accurately represent tubes used in the manufacturing of heat exchangers should be investigated.
- A study into quantifying the maldistribution at the inlet side of the multiple tube heat exchanger should be conducted to optimise tube pitch ratios.
- Higher heat fluxes should be investigated.
- Triangular tube arrangements at varying pitch ratios could be investigated.
- Testing with different fluids would help determine if the observed delay in transition is present at a wider range of Prandtl numbers.

## REFERENCES

- BAKKER, A., LAROCHE, R. D. & MARSHALL, E. M. 2000. *Laminar flow in static mixers with helical elements* [Online]. Available: <http://www.bakker.org/cfmbook/lamstat.pdf> [Accessed 19 July 2017].
- BERNOULLI, D. 1738. *Hydrodynamica sive de viribus et motibus fluidorum commentarii*, Vienna, Austria, Johann Reinhold Dulsecker.
- BYRNE, R. C. 2007. *Standards of the tubular exchanger manufacturers association*, New York, USA.
- ÇENGEL, Y. A. & GHAJAR, A. J. 2014. *Heat and mass transfer: fundamentals & applications*, New York, USA, McGraw-Hill.
- DITTUS, F. W. & BOELTER, L. M. K. 1930. Heat transfer in automobile radiators of the tubular type. *Publications in Engineering*, 2, 443.
- DUNN, P. F. 2010. *Measurement and data analysis for engineering and science*, New York, USA, CRC Press.
- ENERDATA. 2015. *Electricity production* [Online]. Available: <https://yearbook.enerdata.net/world-electricity-production-map-graph-and-data.html> [Accessed July 13 2015].
- FUNG, Y. 1990. *Biomechanics: motion, flow, stress, and growth*, New York, USA, Springer-Verlag.
- GHAJAR, A. J. & TAM, H. K. 2013. Effect of inlet geometries and heating on the entrance and fully-developed friction factors in the laminar and transition regions of a horizontal tube. *Experimental Thermal and Fluid Science*, 44, 680-696.
- GHAJAR, A. J. & TAM, L. M. 1994. Heat transfer measurements and correlations in the transition region for a circular tube with three different inlet configurations. *Experimental Thermal and Fluid Science*, 8, 79-90.
- GHAJAR, A. J. & TAM, L. M. 1995. Flow regime map for a horizontal pipe with uniform heat flux and three different inlet configurations. *Experimental Thermal and Fluid Science*, 10, 287-297.
- GHAJAR, A. J. & TAM, L. M. 1997. Effect of inlet geometry and heating on the fully developed friction factor in the transition region of a horizontal tube. *Experimental Thermal and Fluid Science*, 15, 52-64.
- GNIELINKSI, V. 1976. New equations for heat and mass transfer in turbulent pipe and channel flow. *International Chemical Engineering*, 16, 359-368.
- GOTODA, H. & IZUMI, S. 1978. *A Modern Condenser Design*, Michigan, USA, Institute of Marine Engineers.
- HOLMAN, J. P. 2010. *Heat transfer*, New York, USA, McGraw Hill Higher Education.
- MEYER, J. P. & OLIVIER, J. A. 2010. Single-phase heat transfer and pressure drop of the cooling of water inside smooth tubes for transitional flow with different inlet geometries. *HVAC&R Research*, 16, 471-496.
- MEYER, J. P. & OLIVIER, J. A. 2013. Heat transfer and pressure drop characteristics of smooth horizontal tubes in the transitional flow regime. *Heat Transfer Engineering*, 35, 1246-1253.
- MORCOS, S. & BERGLES, A. 1975. Experimental investigation of combined forced and free laminar convection in horizontal tubes. *ASME Journal of Heat Transfer.*, 97, 212-219.
- NUSSELT, W. 1915. Das grundgesetz des wärmeüberganges. *Gesundheits-Ingenieur*, 38(42), 477-482. 490-496.
- PEREZ, R. 2013. *A way to the most abundant energy* [Online]. Available: <https://www.scientificamerican.com/article/a-way-to-the-most-abundant-energy/> [Accessed 11 July 2017].
- POPIEL, C. O. & WOJTKOWIAK, J. 1998. Simple formulas for thermophysical properties of liquid water for heat transfer calculations. *Heat Transfer Engineering*, 19, 87-101.
- REYNOLDS, O. 1883. On the experimental investigation of the circumstances which determine whether the motion of water shall be direct or sinuous, and the law of resistance in parallel channels. *Philosophical Transactions of the Royal Society of London*, 174 935-82.



- SHAH, R. K. & SEKULIC, D. P. 2003. *Fundamentals of heat exchanger design*, New Jersey, USA, John Wiley & Sons.
- STOKES, G. G. 1851. On the effect of the internal friction of fluids on the motion of pendulums. *Cambridge Philosophical Transactions*, IX.
- UNPF. 2015. *World population trends* [Online]. United Nations Population Fund. Available: <http://www.unfpa.org/world-population-trends> [Accessed July 13 2015].
- WHITE, F. M. 2003. *Fluid mechanics*, New York, USA, McGraw-Hill.



# Appendix A CALIBRATION

## 1. INTRODUCTION

This appendix discusses the process of PT100 and thermocouple calibration used in determining the heat transfer results presented in this dissertation. The results of the calibration are also presented.

Both the PT100 probes and the T-type thermocouples exhibit a linear relationship with increasing temperature, and thus a linear regression analysis was used to determine the calibration coefficients for the sensors. The output of each sensor is plotted against a reference value, and the slope and intercept of the best fit line through the data points is used as the calibration equations.

## 2. PT100 CALIBRATION

The PT100 probes were calibrated using a Lauda Proline thermal bath, capable of maintaining a set temperature with a stability of 0.02°C. The reference used for the calibration was a Lauda DigiCal which has an accuracy of 0.03°C and was factory calibrated.

The PT100 probes were connected to the National Instruments data acquisition system and the thermal bath was set to 15°C. Once the system had reached stable conditions and the fluctuations on all probes had disappeared, a total of 100 data points were logged. This process was repeated in increments of 2.5°C up to a maximum of 67.5°C and back down using the same decrements to 15°C. This process was then repeated three times as suggested by Dunn (2010) to evaluate the precision of the calibration and prove repeatability.

The average of each 100-point data sample was then plotted against the reference temperature as shown in Figure A.1.

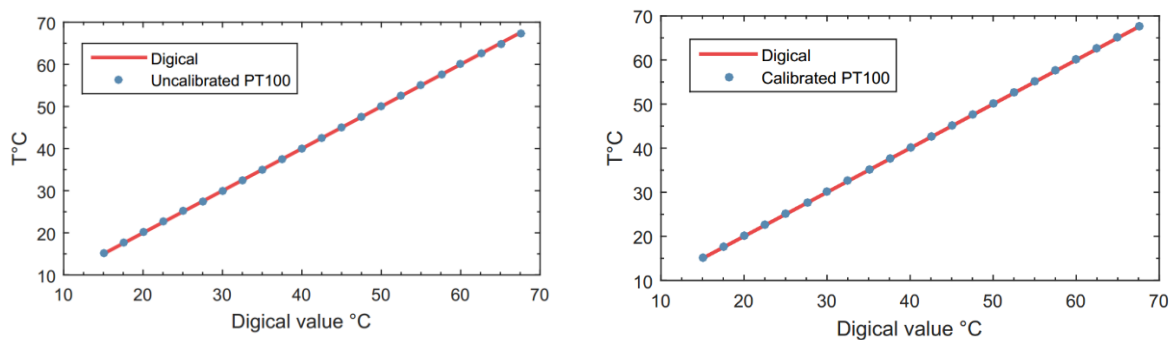


Figure A.1. Response of the PT100 probe against the DigiCal reference before calibration (left) and after calibration (right).

The linear regression analysis was used to determine the equations for the calibration of the PT100 probes, and the residual (error) of the PT100 before and after applying the equation coefficients is plotted as shown in Figure A.2 to visually analyse the precision of the calibration.

The calibration equation coefficients that were determine for each PT100 probe are given in Table A.1.

Table A.1. Slope and intercept of the calibration equations for the inlet and three outlet PT100 probes.

	<i>Slope</i>	<i>Intercept</i>
<i>Inlet PT100</i>	0.9996	0.0126
<i>Outlet PT100 right</i>	1.0022	-0.0861
<i>Outlet PT100 centre</i>	1.0014	-0.0337
<i>Outlet PT100 left</i>	1.0042	-0.0673

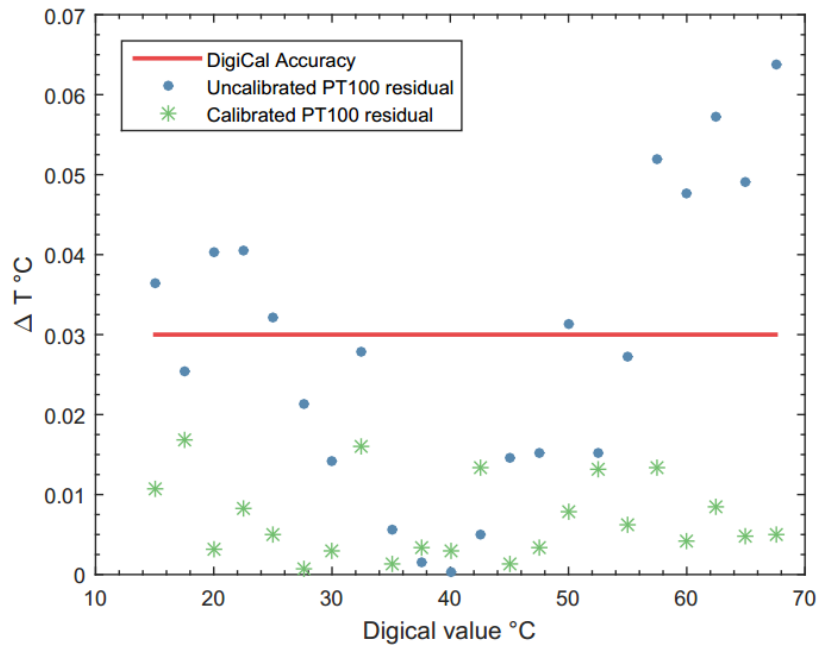


Figure A.2. Uncalibrated and calibrated residuals of the PT100 against the DigiCal reference.

### 3. THERMOCOUPLE CALIBRATION

An in-situ approach to the calibration of the thermocouples was used to negate any effect the attachment method may have on the calibration equation coefficients. The T-type thermocouple junctions were made by soldering the ends of the thermocouple wire with tin solder. These junctions were then inserted into the indentations drilled into the outer surface of the test tubes and fastened in place using a high conductivity thermal epoxy.

The supply and return lines of the Lauda Proline thermal bath were then connected to the inlet and outlet of the test tubes. The calibrated PT100 probes were placed at the inlet and outlet of the tube to measure the bulk fluid temperature through the test section. An identical approach to the calibration of the PT100 probes was then repeated in intervals of 2.5°C from 17.5°C up to a maximum of 65°C. Measurements of 100 data points were then taken for the same decrements back down to 15°C and the process was repeated three times as suggested by Dunn (2010).

The linear regression analysis was used to determine the equations for the calibration of each thermocouple, and the response of each thermocouple before and after applying the equation coefficients is plotted as shown in Figure A.3 to visually analyse the precision of the calibration.

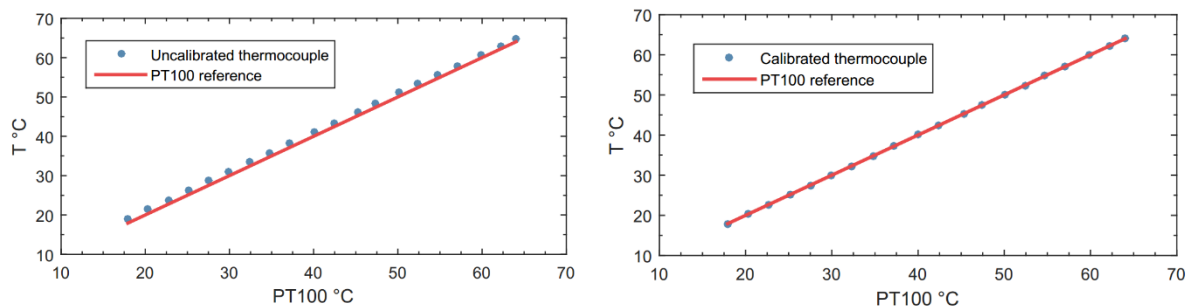


Figure A.3. Response of a sample thermocouple against the PT100 reference before calibration (left) and after calibration (right).



The linear regression analysis is used to determine the equations for the calibration of each thermocouple, and the residual (error) of each thermocouple before and after applying the equation coefficients is plotted as shown in Figure A.4 to visually analyse the precision of the calibration.

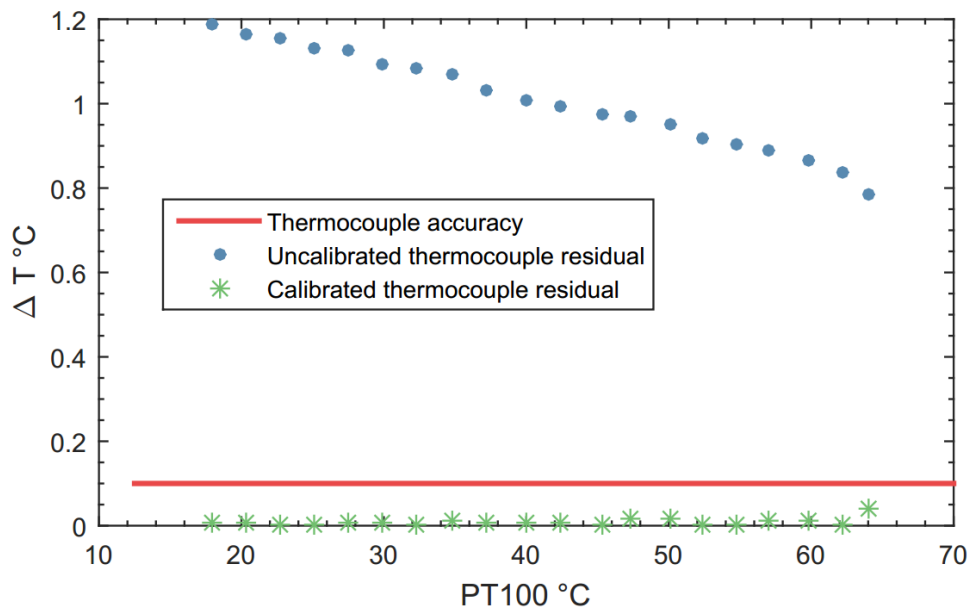


Figure A.4. Uncalibrated and calibrated residuals of a sample thermocouple against the PT100 reference.

Table A.2 shows the coefficients of the equation of a sample thermocouple used for this analysis.

Table A.2. Slope and intercept of the calibration equation for the sample thermocouple.

	<i>Slope</i>	<i>Intercept</i>
<i>Sample thermocouple</i>	1.0081	-1.3488

#### 4. CONCLUSION

Appendix A describes the calibration process followed for the calibration of the temperature sensor equipment – namely the PT100 probes and the T-type thermocouples. Through the calibration process the sensors were found to be calibrated to within their respective accuracies. This provides confidence in the results obtained in the results section of this dissertation.

## Appendix B UNCERTAINTY

### 1. INTRODUCTION

This appendix discusses the method of calculating the uncertainty associated with the investigation in this dissertation. A sample calculation is shown and demonstrates the calculation process followed for calculation of subsequent uncertainties.

### 2. REYNOLDS NUMBER

To calculate the uncertainty for Reynolds number, the uncertainties for mass flow rate, inner diameter and dynamic viscosity are required. To determine the uncertainty of mass flow rate, the method proposed by Dunn (2010) was used. The precision was obtained by multiplying the standard deviation across 200 data points with Student's t-variable and the bias was obtained from manufacturer specification.

$$\begin{aligned}\delta\dot{m} &= (b_i^2 + p_i^2)^{0.5} \\ \delta\dot{m} &= ((1.1333 \times 10^{-5})^2 + (1.980 \times 3.5401 \times 10^{-6})^2)^{0.5} \\ \delta\dot{m} &= 1.3325 \times 10^{-5}\end{aligned}$$

The inner diameter and fluid property uncertainty values are given as:

$$\begin{aligned}\delta D_i &= 3.8 \times 10^{-5} \\ \delta \mu_b &= 0.01 \cdot \mu_b = 8.425 \times 10^{-6}\end{aligned}$$

The Reynolds number uncertainty can be calculated as follows:

$$\begin{aligned}\delta Re &= \frac{4}{\pi} \left[ \left( \frac{1}{\mu_b D_i} \delta \dot{m} \right)^2 + \left( -\frac{\dot{m}}{\mu_b^2 D_i} \delta \mu_b \right)^2 + \left( -\frac{\dot{m}}{\mu_b D_i^2} \delta D_i \right)^2 \right]^{0.5} \\ \delta Re &= \frac{4}{\pi} \left[ \left( \frac{1}{8.425 \times 10^{-4} \cdot 0.004} \cdot 1.3325 \times 10^{-5} \right)^2 + \left( -\frac{0.011099}{(8.425 \times 10^{-4})^2 \cdot 0.004} \cdot 8.425 \times 10^{-6} \right)^2 \right. \\ &\quad \left. + \left( -\frac{0.011099}{8.425 \times 10^{-4} \cdot 0.004^2} \cdot 3.8 \times 10^{-5} \right)^2 \right]^{0.5} = 58.05\end{aligned}$$

A Reynolds number of 4193.1 was used, thus the uncertainty for Reynolds number was 1.38%.

### 3. CONCLUSION

A sample calculation for the uncertainty for Reynolds number is provided for a single data point. The complete list of uncertainties is summarised graphically in Section 3.9. A similar process as proposed by Dunn (2010) was followed in calculating the uncertainties for any other parameter mentioned in this dissertation.